NASA Contractor Report XXXXXX

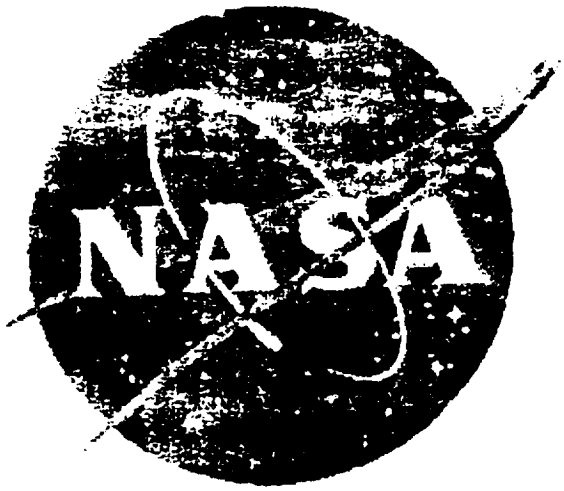

Grant NAG1-1376

STRUCTURAL QUALIFICATION OF COMPOSITE AIRFRAMES

Keith T. Kedward and John E. McCarty
Department of Mechanical and Environmental Engineering
University of California at Santa Barbara
Santa Barbara, CA 93106-5070

August 1995
2nd Draft Sent March 1997

National Aeronautics and
Space Administration
Langley Research Center
Hampton, Virginia 23681-0001

ABSTRACT

The development of fundamental approaches for predicting failure and elongation characteristics of fibrous composites are summarized in this document. The research described includes a statistical formulation for individual fiber breakage and fragmentation and clustered fiber breakage, termed macrodefects wherein the aligned composite may represent a structural component such as a reinforcing bar element, a rebar. Experimental work conducted in support of the future exploitation of aligned composite rebar elements is also described. This work discusses the experimental challenges associated with rebar tensile test evaluation and describes initial numerical analyses performed in support of the experimental program.

Contents

1.0 INTRODUCTION

Previous research that established a fundamental foundation for developing models and methods for predicting the strength and elongation of fibrous composites was presented by Palmer (1981). This work was further developed in the Phase 2 effort described herein. A primary objective of this collective effort has been to develop models that may be used to predict the strength and elongation of fibrous composite systems from a knowledge of the basic properties of the constituent fiber and matrix materials. It is now widely recognized that the sequential breakdown of the fiber and matrix constituents and the associated interface precludes the reliable application of the well known mixture rule for stress in a composite material, i.e.,

$$\bar{\sigma} = f s_f + (1 - f) s_m \tag{1.1}$$

It is also known that some form of statistical foundation, typified by some form of Weibull theory, can be valuable in obtaining predictions and insight into the subtle manner in which fibrous composites accumulate progressive damage under uniaxial loading. In this work, we extend the treatment to flexural loading considered to represent failures that might result from local bending of rebar elements following complete breakdown and loss of support from a surrounding concrete material. The treatment is intended to address the concern over catastrophic failure that could result

from the abrupt failure of rebars in reinforced concrete waterfront structures following earthquake, extensive wave activity or blast loading.

The current range of high performance composites used extensively in aerospace structural components are known to have ultimate strains-to-failure in the 1 to 2% range and typical allowable tensile strains of less that 0.5%. In civil engineering applications, such a low strain capability could be a major impediment, particularly in view of the desire to avert catastrophic failures and consequent separation of structural components. Thus, the thrust of the current research is to provide models and methods that will aid in evaluation of the potential structural merits of the wide range of composite systems and constituent fibers and matrices.

To complement the above theoretical studies, a parallel experimental effort executed in close collaboration with the Naval Facilities Engineering Service Center (NFESC), Port Hueneme, has provided data on reinforcing bars and prestressing strands for reinforced and prestressed concrete structures. These bars and strands were supplied to the University of California at Santa Barbara (UCSB) by NFESC as were the generous use of NFESC's experimental facilities. As part of the experimental studies, detailed numerical (finite element) analyses were also conducted on gripping methods and end anchorages. It is a frequent experience in such investigations for induced stress concentrations in the vicinity of the grips to precipitate premature failures, thereby limiting the extent of representative data collected. This was the case again experienced, although considerable progress was made in developing and understanding the mechanisms responsible for premature grip failure and resulting

modifications in grip/attachment design. Of course, the high degree of anisotropy inherent in most polymer matrix composites (PMC) contribute a greater level of complexity, and a resulting need for a more thorough fundamental background, that motivates such studies.

2.0 EXPERIMENTAL PROGRAM ON STRENGTH

This section describes the experimental program conducted to determine the applicability of various materials for use as replacements for standard steel rebar in naval ocean, waterfront and facility structures. Current materials, while adequate in the initial design and construction phases of operation, have an inherent life limitation brought about by both fatigue of the structure and corrosion of the material due to an adverse environment, in this case saltwater exposure. The use of composites offers a potentially viable solution to these problems. The fatigue life of some composite systems can be considerably higher, and composites can be constructed to be resistant to the rigors of a marine environment. This study looks at both metal matrix composites (MMC) and polymer matrix composites (PMC) as improvements to the current steel standard. This approach affects a sound fundamental understanding of the micro-mechanical mechanisms inherent in these systems. The comparison of the basic differences between such rigid and flexible matrix materials can provide valuable insight into designing composite structures. The research also focuses on the failure modes of these materials. Current steel rebar fails in a ductile fashion. The bar will stretch with increased load causing a visible crack in the encasing concrete. This crack allows warning and repair before catastrophic failure of the structure occurs. Unlike steel, some contemporary composites tend to fail in a catastrophic manner. This research attempts to balance the inherent benefits of fatigue life and environmental

resistance and the constraints of catastrophic failure inherent in composite materials to create an alternative to steel rebar that potentially offers a lower lifetime cost.

2.1 Ultimate Strength and Elongation of MMC Systems

The first section of the study examines the use MMC's with a focus on creating a model to predict the ultimate strength of the material. The material used in this study was a unidirectional $[0°]_4$ titanium matrix composite, SCS6/Ti 15-3 made by Textron. It consisted of 38% SiC fibers in a matrix composed of a metastable β-Ti alloy. Because of the still limited availability of titanium MMC's, three specimens of each type were used to determine the mean strength for each configuration. Various tests were completed to characterize the material and examine the volume dependence of the strength of the material. Tension, three-point and four-point bending tests were conducted to determine the ultimate strength of the material under various loading conditions. Other experiments included, examining the in situ fiber characteristics to determine the differences between pristine fibers and extracted fibers, and a series of notch tests to determine the notch sensitivity and other fracture parameters.

Specimens with a reduced gauge section were used to determine the tensile strength. Two specimens with gauge lengths of 10 mm and 200 mm and a transition radius of 2 inches were used to determine the volume dependence of the tensile strength as shown in Figure 2.1. This radius has been shown to be sufficient to cause failures, predominantly in the gauge section, for this type of composite [Jansson et al, 1991].

Figure 2.1
Reduced Gauge Section Specimens

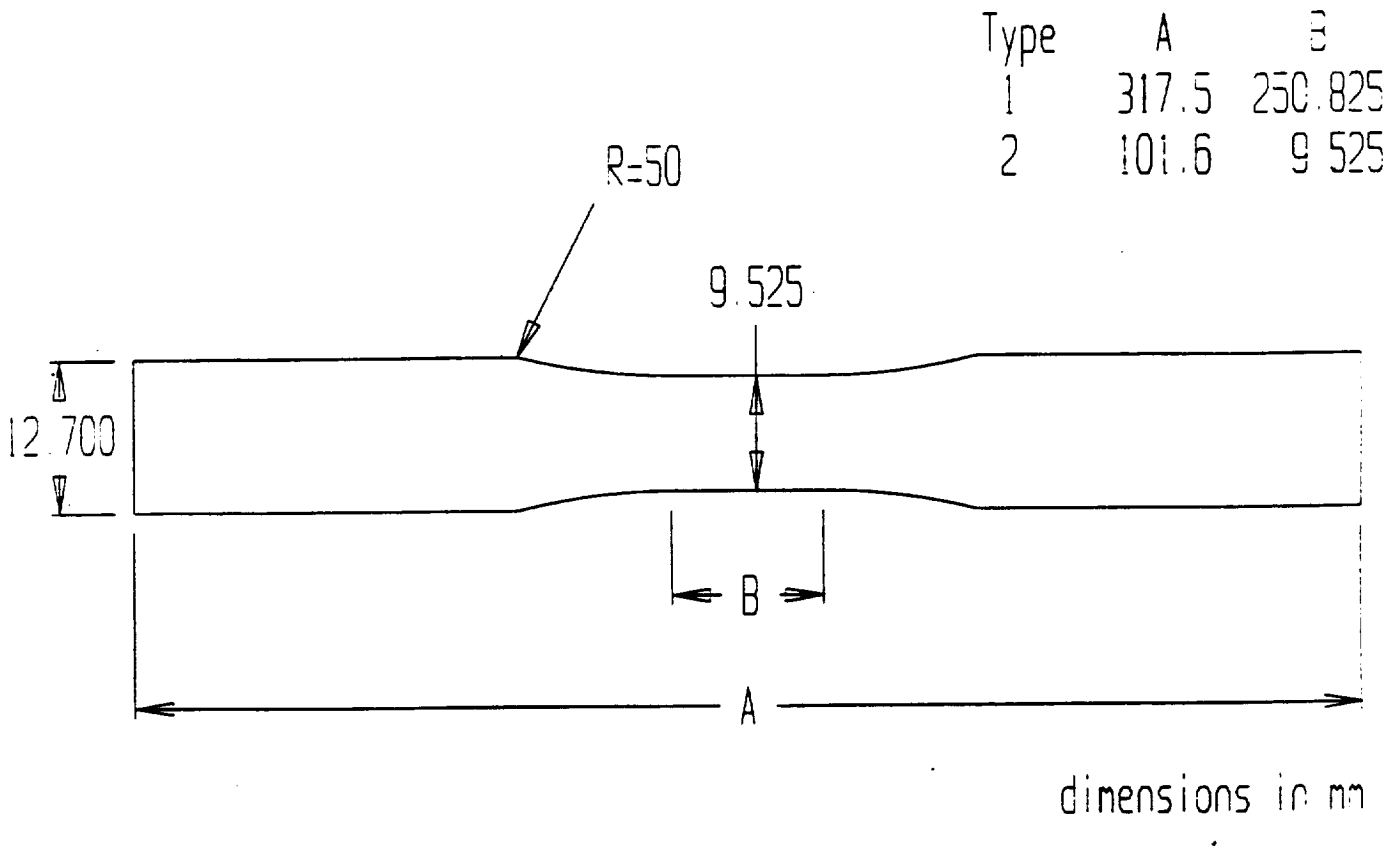

Figure 2.1. Reduced gauge section specimens used for tensile testing.

The specimens were loaded in a servo-hydraulic test system using wedge grips and the strain was measured with an extensometer having a 6-mm gauge length. The tensile response exhibited an initial linear response with a slight decrease in slope after matrix yield. The final failure was catastrophic and the long specimens had sufficient stored energy to cause secondary bending failures after the initial tensile failure, as shown in Figure 2.2. The test results indicated a slight variation in strength for each specimen length and the average strength for the long specimens was slightly lower than that of the short specimens [Bish, Jansson, Kedward, 1996].

Three- and four-point bending tests were performed using standard fixtures illustrated in Figures 2.3 and 2.4, respectively. Span lengths of 20 mm and 90 mm were used for the three point bending tests. The four-point bending tests were conducted with a center span length of 20 mm. The bending tests were performed in an electro-mechanical screw-driven system and the reported displacement is the ram displacement [Bish, Jansson, Kedward, 1996].

Four-point bending tests were performed on specimens with a rectangular cross section. The bending response exhibited some initial slack and was linear thereafter up to the final catastrophic failure. The failure was initiated on the tensile side of the beam. In some cases, the crack arrested and the displacement had to be increased at a lower loading level than for the initial failure to cause the final separation, as shown in Figure 2.5. The nominal bending strength was higher than the tensile strength of the composite while the specimen-to-specimen variation was of the same magnitude [Bish, Jansson, Kedward, 1996].

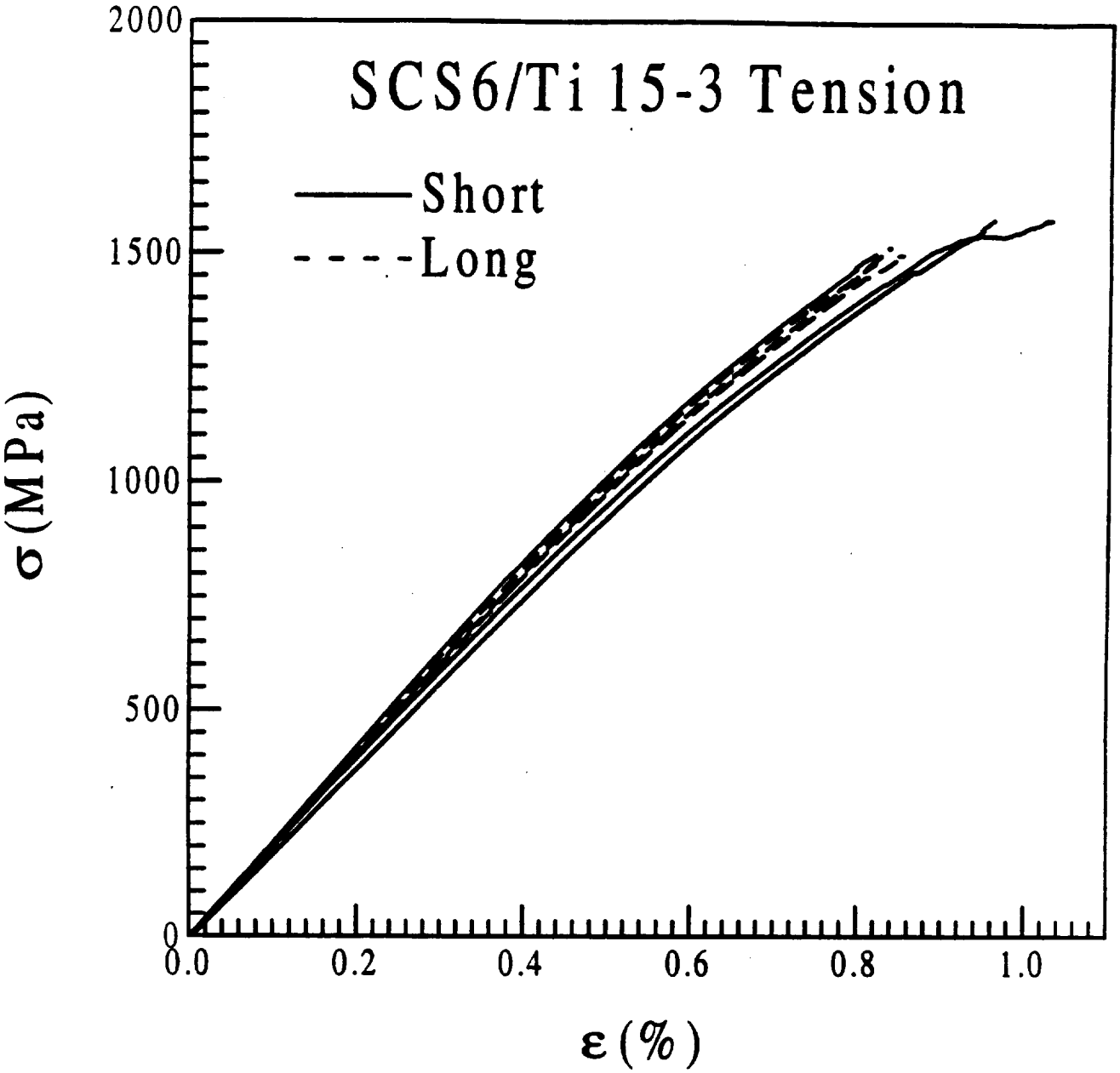

Figure 2.2. Longitudinal tensile responses.

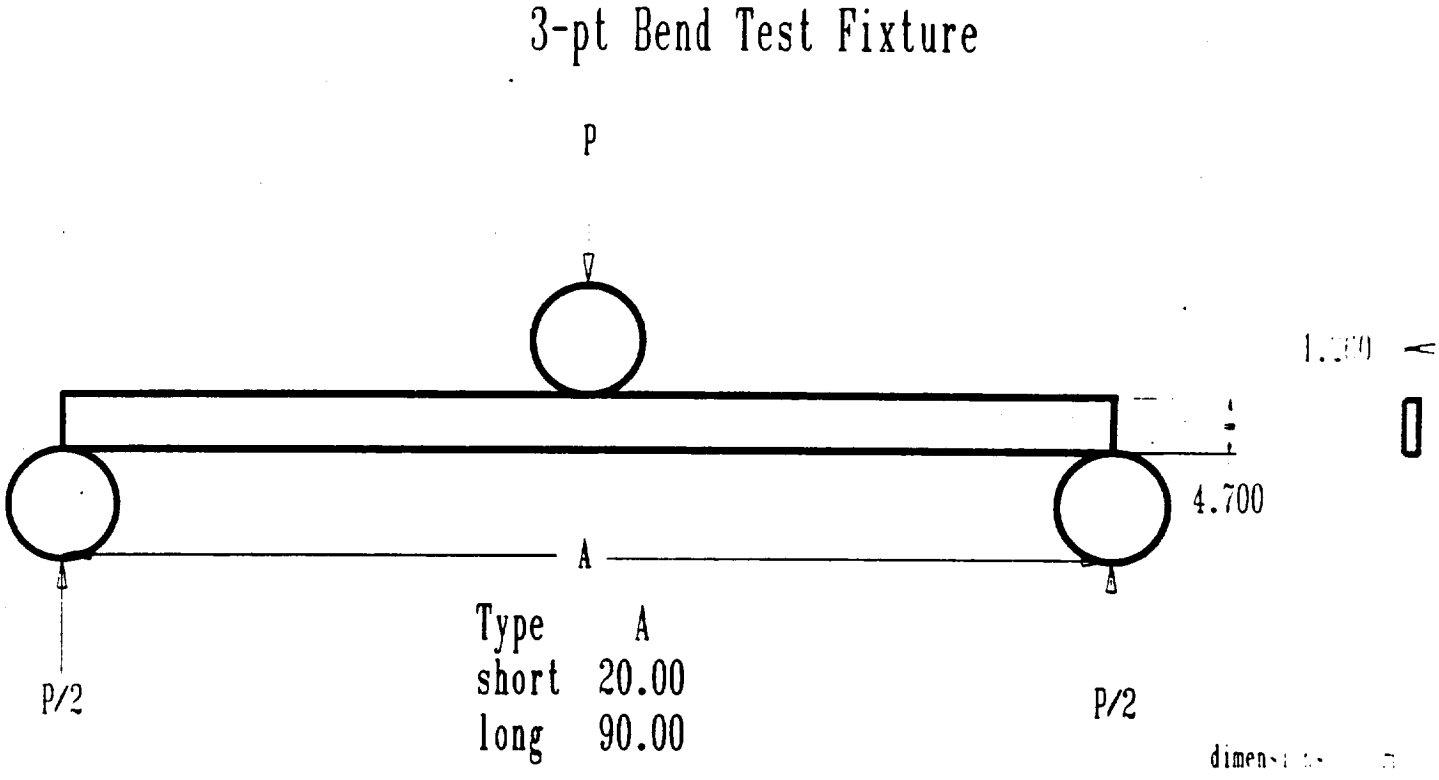

Figure 2.3. Three-point bend test fixture.

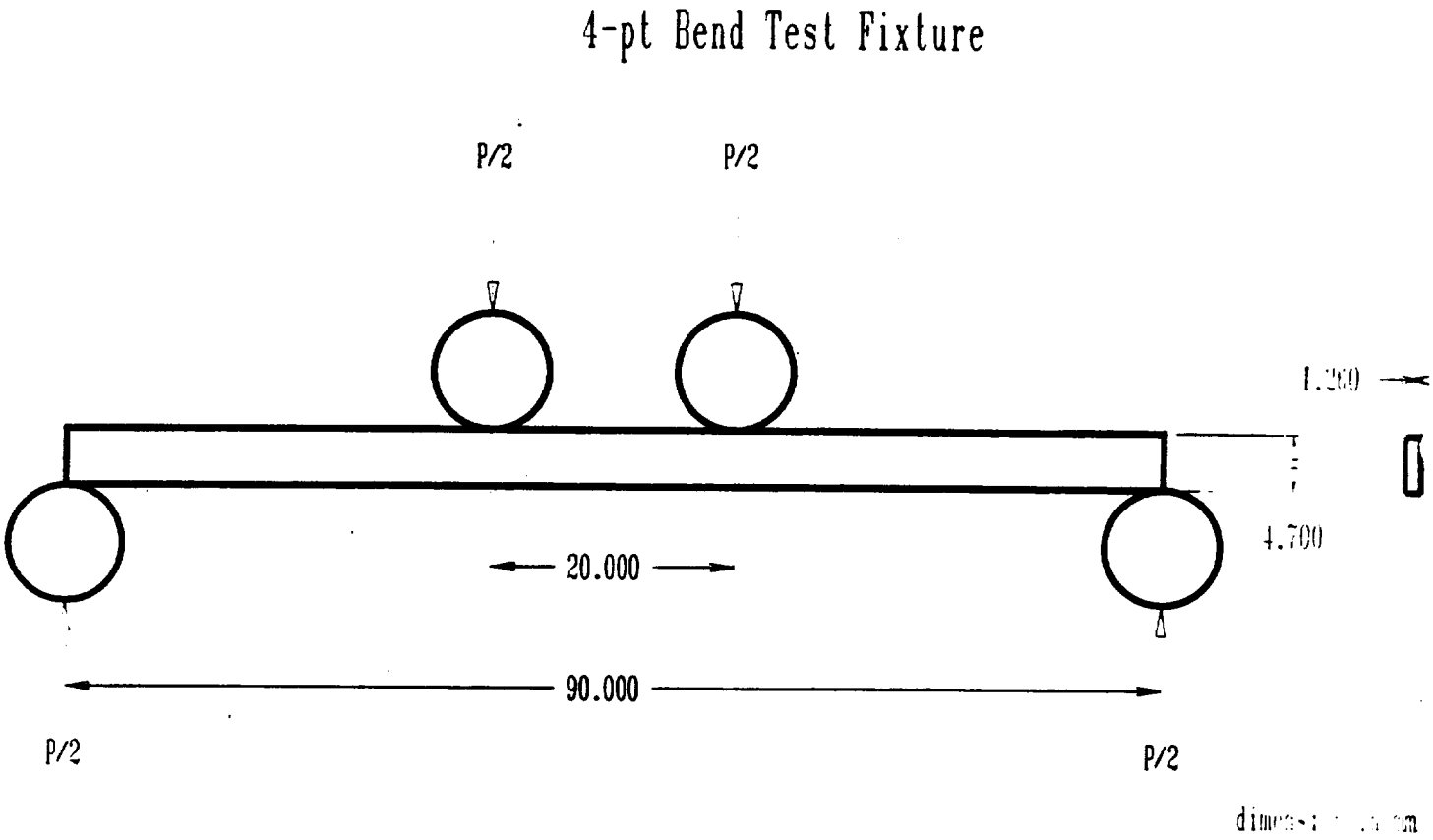

Figure 2.4. Four-point bend test fixture.

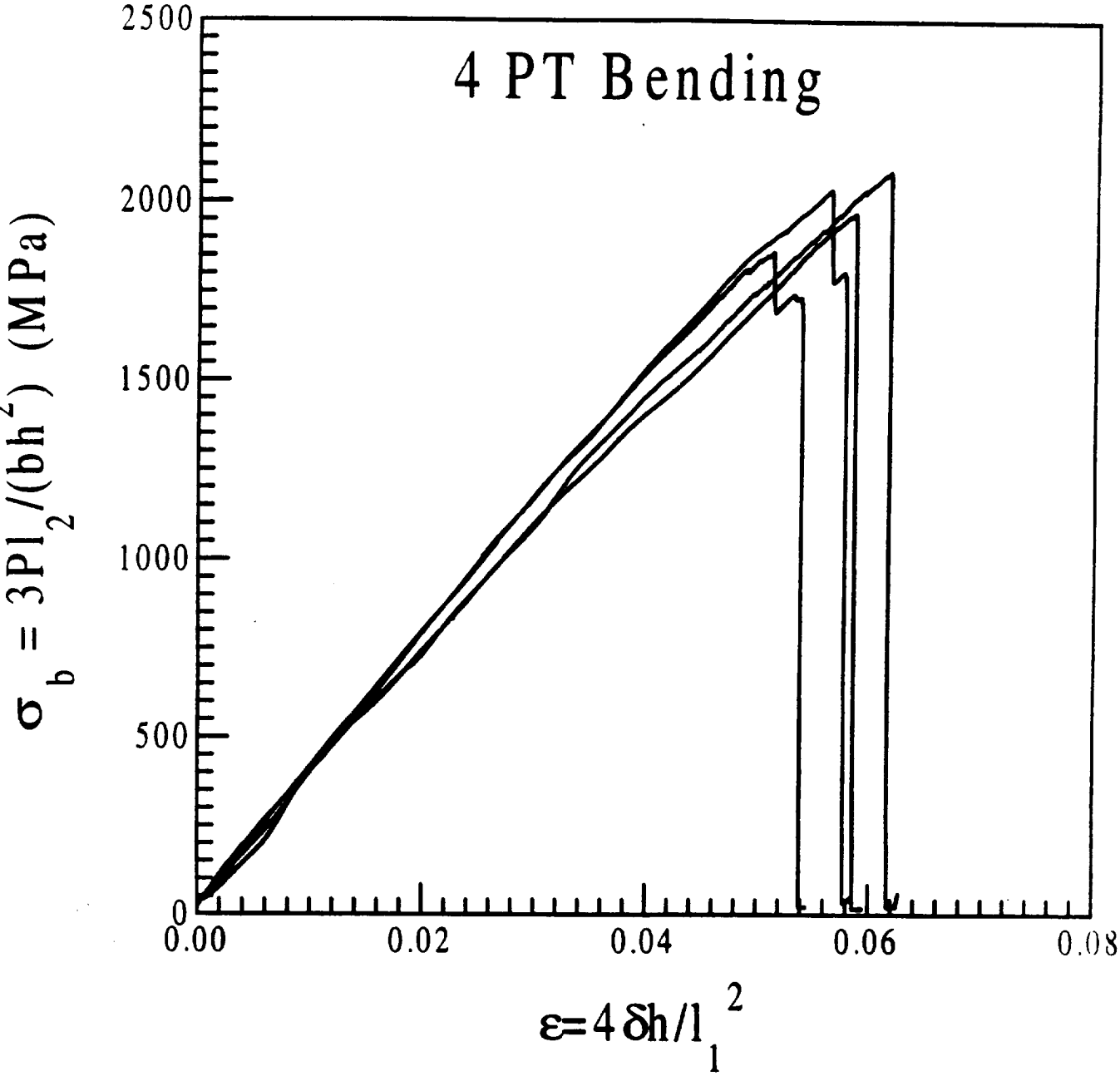

Figure 2.5. Normalized load deflection relationships for four-point bending tests.

Three-point bending tests were performed on rectangular beams with two different lengths. The response of the long beams were linear up to a catastrophic failure with a load drop to zero load. The long beams were more flexible and had sufficient stored energy to drive the fracture to a full separation as shown in Figure 2.6. The response for the short beams was more stable and the initial failure was followed by controlled separation under decreasing load after the initial load drop, as seen in Figure 2.7. The strength in shorter three-point bending specimens was higher than for longer three-point bending specimens. The strength in the three-point bending tests was also higher than in four-point bending tests. The sample-to-sample variation was of the same order as in the previous tests [Bish, Jansson, Kedward, 1996].

To assess the flaw sensitivity of the material, tests using double-edged notched specimens were performed. The notches were cut by using a diamond blade saw with a thickness of 0.2 mm. The specimen width was 8 mm and the ratio of notch length to specimen width was 0.15, as illustrated in Figure 2.8. The results show that the nominal stress, in the ligament between the two notches, was slightly lower than the tensile strength of the short specimens. This indicates a notch weakening. The fracture toughness was approximately K_I = 55 MPa$\sqrt{m}$ [Bish, Jansson, Kedward, 1996]. This result compares favorably with the simple model by Kelly and Tyson [1965] in which it is assumed that the toughness is given by the plastic dissipation in the matrix. This model predicts a toughness of 50 MPa$\sqrt{m}$. Another series of notch tests were completed using various crack length to specimen width ratios. The results

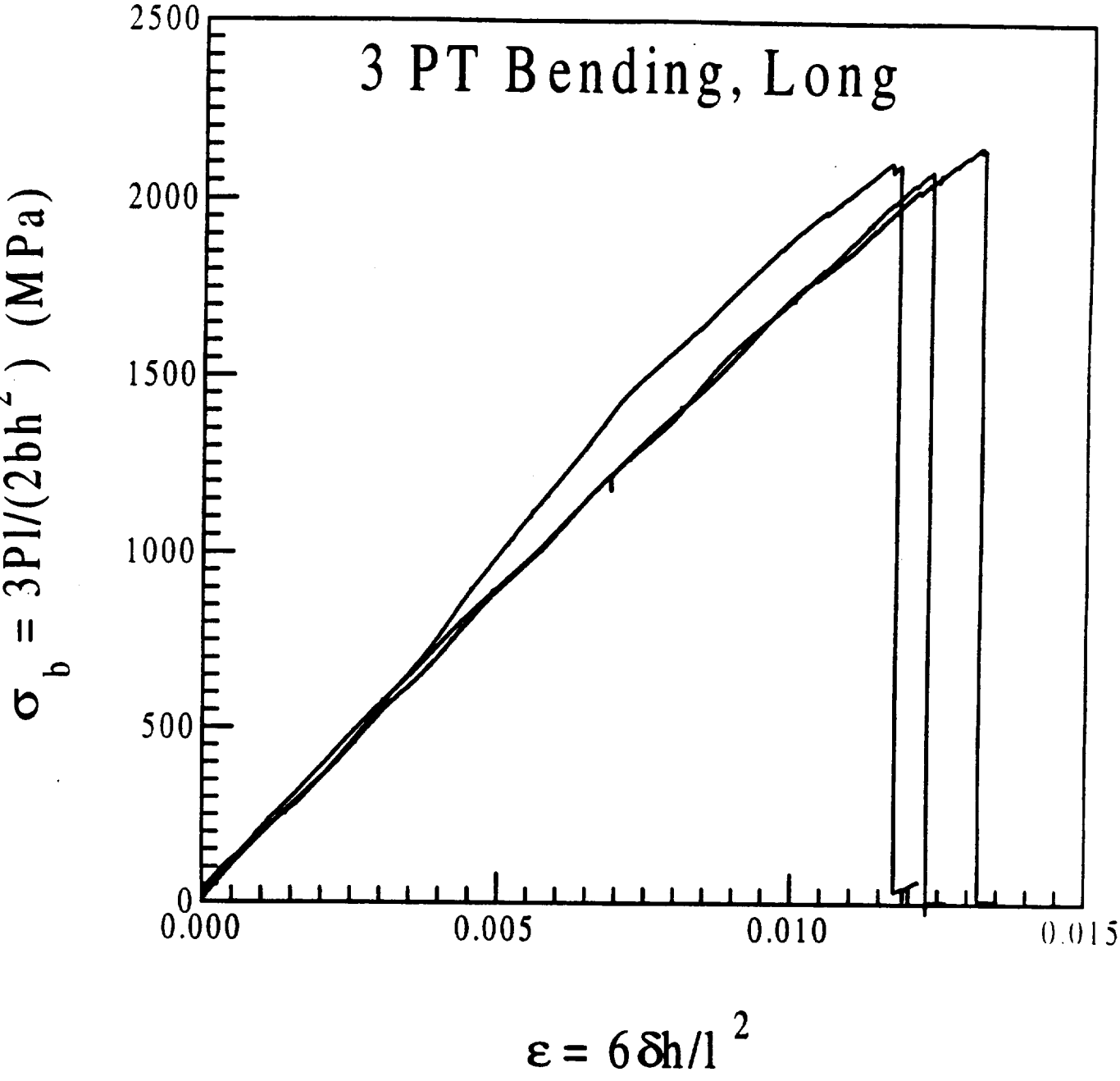

Figure 2.6. Normalized load deflection relationships for long-three point bending tests.

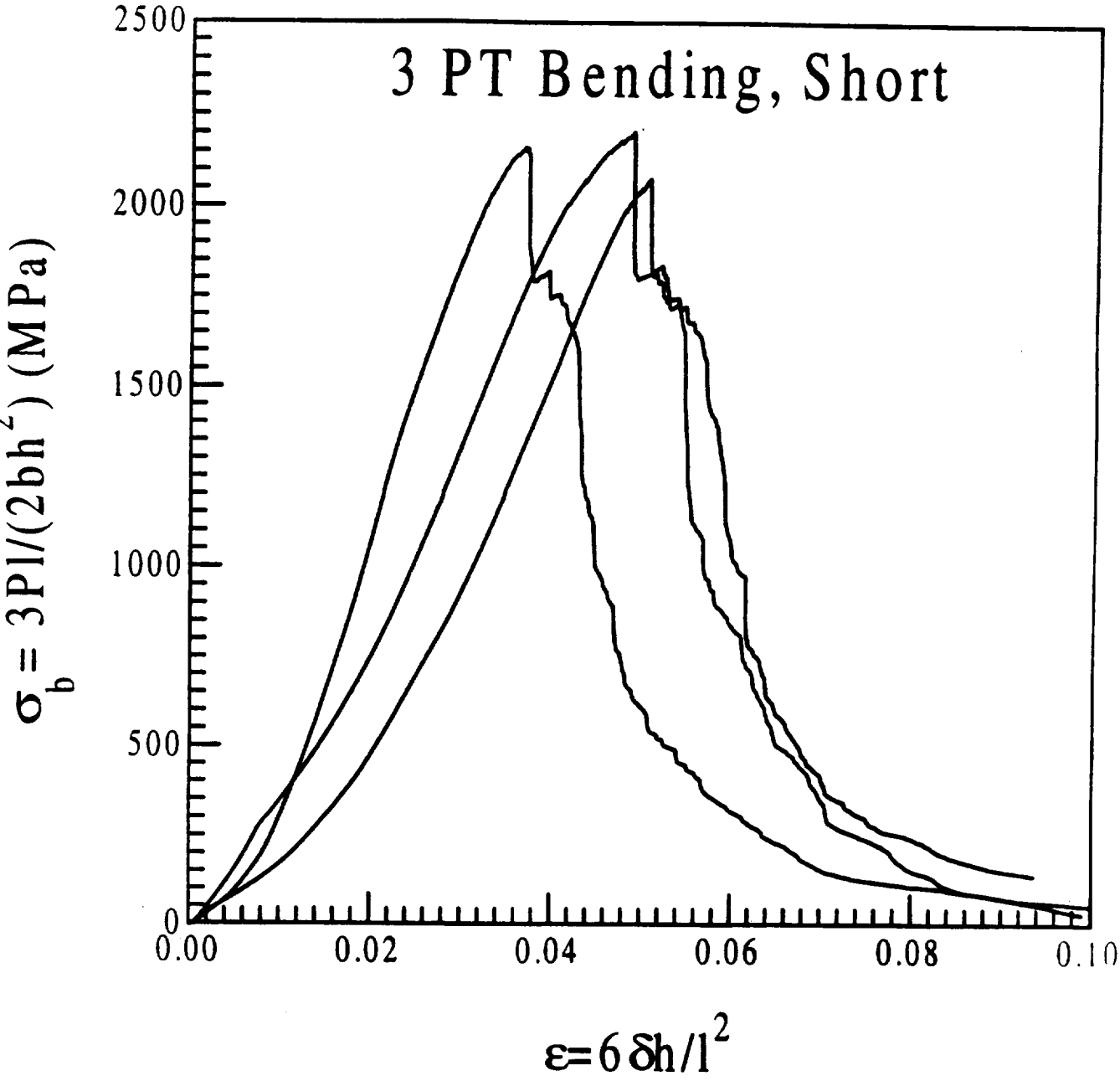

Figure 2.7. Normalized load deflection relationship for short three-point bending tests.

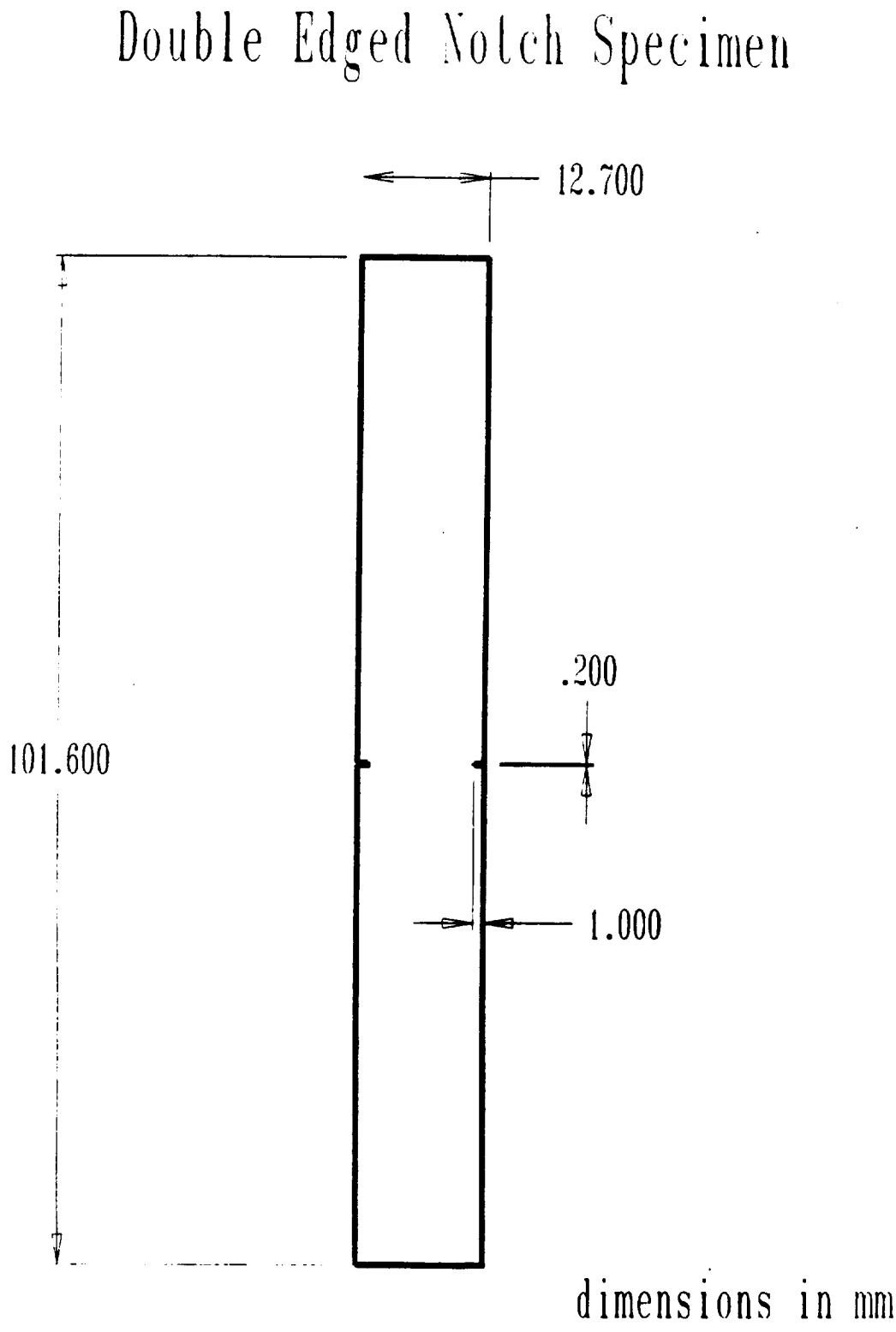

Figure 2.8. Specimen used to assess fracture toughness for short cracks.

of this series of tests will eventually be used in the creation of a predictive model examining the effects of notches on the ultimate strength of this material.

The final test series performed on the MMC's was to determine the fiber properties in the manufactured material. The fiber modulus for the SCS6 fibers has been reported to be in the range of 360 to 400 GPa. The fiber strength is length dependent and is usually given in terms of a mean strength and a Weibull modulus. A mean strength of 4.3 GPa and a Weibull modulus of 9.3 has been reported for pristine fiber with a length of 50 mm [Bain et. al, 1985]. To determine the in situ fiber strength for the present composite, 100 fibers were extracted from the composite by etching the matrix away using a 49 percent HF solution. A few initially broken fibers were found in the composite. The average strength for the extracted fibers was 3.65 GPa and the Weibull modulus was 4.9, as shown in Figure 2.9, [Bish, Jansson, Kedward, 1996]. This indicates that a substantial degradation occurs during the fabrication of the composite.

2.2 Ultimate Strength and Elongation of PMC Systems

The second section of this study focuses on PMCs. The experimental research in this section deals with creating an effective grip, so that the strength of composite bars can be accurately determined. Traditional gripping mechanisms have proven unsatisfactory in determining the tensile strength of composite rebars due to the induced stress concentrations near the end of the grips which initiate a premature

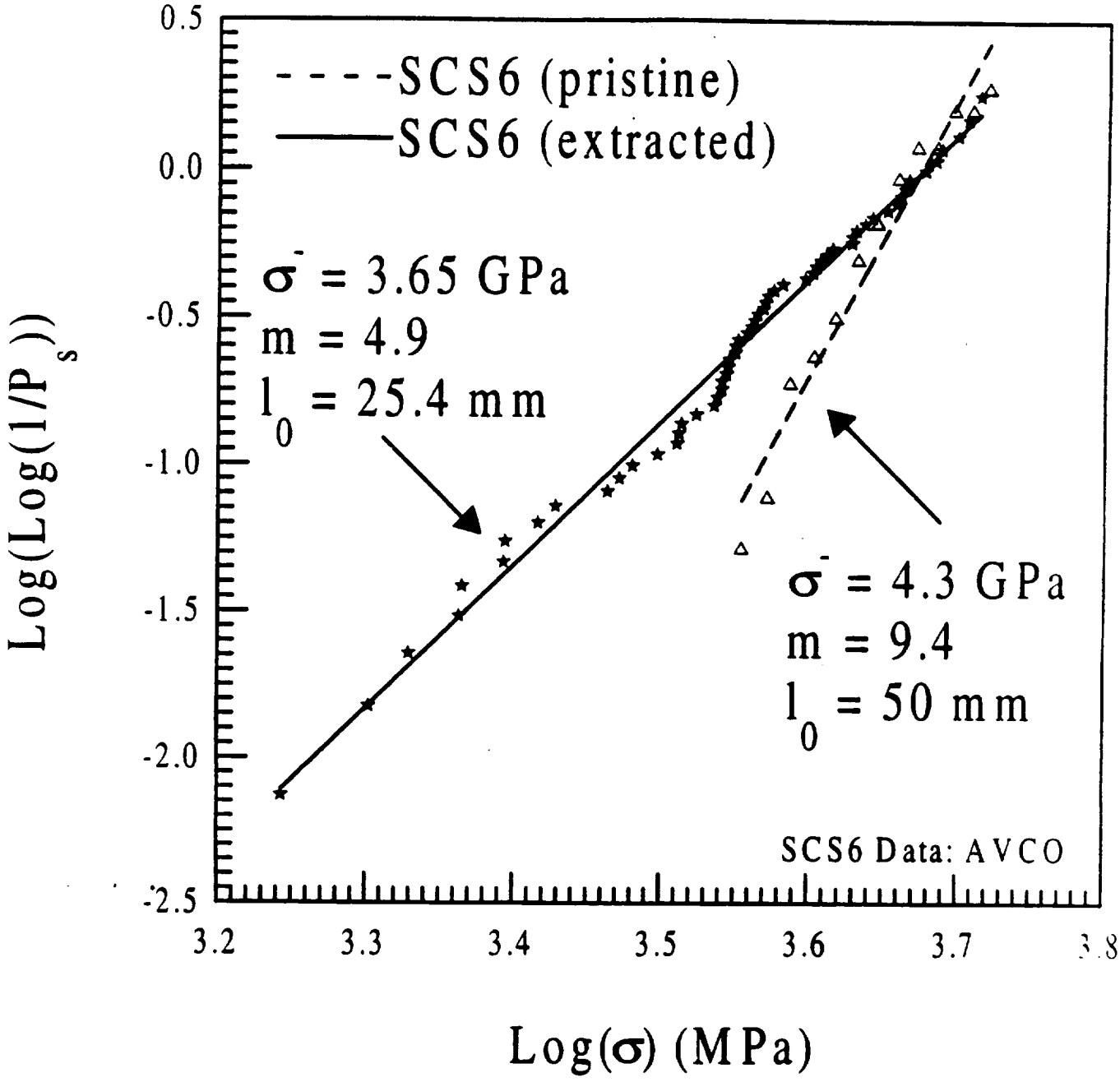

Figure 2.9. Weibull plot of the strength of pristine fibers and fibers extracted from the composite.

failure. In this project, two types of clamping mechanisms were examined experimentally in order to solve this problem. The first method is the clamp, in which the rebar is held between four blocks fastened together by bolts. The second method is the end wrap in which the rebar is wrapped with another material, usually with a higher strain to failure than the rebar that is used to protect the test specimen.

The use of clamp grips and end wraps was examined as a means of alleviating the increasing strain in the rebar adjacent to the bar/grip interface and the stress concentration near the end of the clamp grips. The strain in the bar increased with increasing radius with the maximum strain at the outer radius of the bar, but the strain profile smoothed out as the distance from the grip end increased [Malvar, Bish, 1995]. These problems occurred in the clamp grip, four aluminum blocks bolted together with a specified level of lateral pressure, and in standard grips, ASTM tab adapters, even though an increase in strength was noted with the use of the clamp grips. The predominant failure mode in the clamp grips was still caused by the high strain level at the rebar/grip interface. By wrapping the bars with a material capable of handling high elongations, this problem can be alleviated. Wrapping the bars with more layers of E-glass was insufficient because, although the high strain levels had been removed from the rebar, the strain level was still present in the wrap which fails causing failure of the bar. Addition of a different material that can withstand higher strain levels should solve this problem, provided the material is capable of high enough elongation. The effects on the strain distribution caused by the addition of both stiff and flexible wraps is illustrated by the finite element results presented in Figure 2.10. In this figure, the

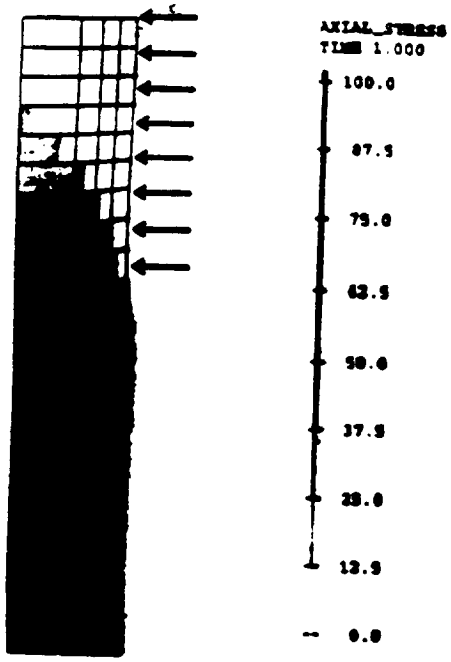

Figure 2.10a. Stress concentration.

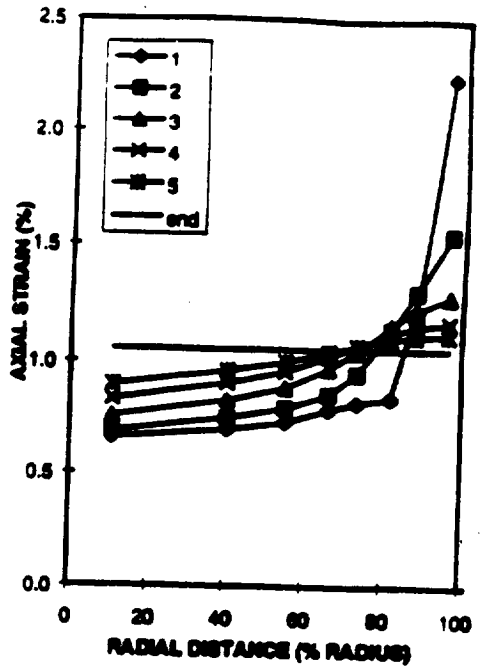

Figure 2.10b. Radial strain distribution near the grips end

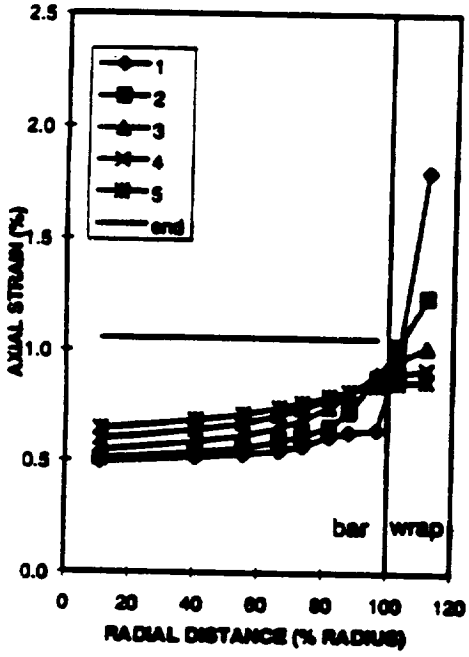

Figure 2.10c. Radial strain distribution stiff wrap

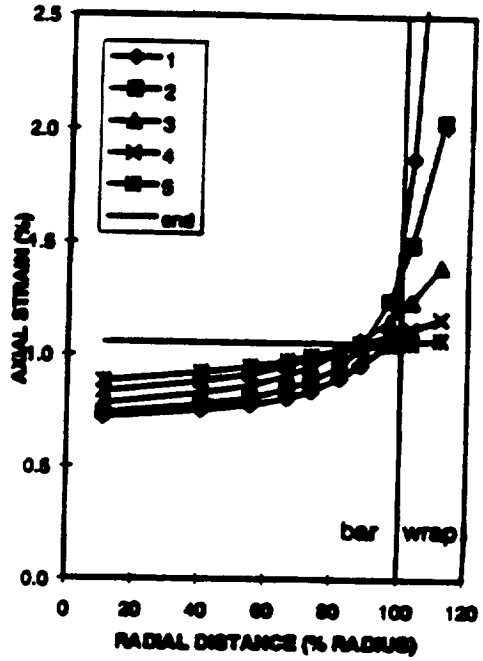

Figure 2.10d. Radial strain distribution flexible wrap

Figure 2.10. Finite element results for the radial strain distribution near the end of the grip with and without end wraps.

axial strain is plotted against the distance from the bar center for the first five (1-5) layers of elements below the grips.

The majority of the current work on these types of gripping mechanisms focuses on small diameter rods from 3.2 mm [Holte, Dolan and Schmidt, 1993] to 8 mm [Sippel, 1992], and [Iyer, Anigol, 1991]. This diameter is considerably smaller than the 19 mm (.75 in) standard rebar examined in this study. The increase in size causes premature rupture in the outer layers of the specimens creating an apparent size effect due to the increased shear lag in the larger specimens.

Different kinds of PMC rebar were examined in the course of this study. A hybrid, carbon/E-glass bar, and two kinds of E-glass bars which from previous work have been shown to be well behaved. The hybrid bars consisted of an E-glass core surrounded by an outer layer of carbon and E-glass at an angle. The hybrid bars were tested using various end wraps, a carbon acrylic composite, soft copper tubing, fiberglass, and various epoxies in an attempt to add more compliance to the system by increasing the elongation near the bar/grip bar interface. The tests were showing sporadic results, not due to the methods, but because of the bars. Close examination of the bars, especially the failed specimens, showed extensive manufacturing variability in the rebar. These imperfections included distortion of the rebar and inconsistent thickness of the outer wrapping. These flaws caused premature failure of the bars. The distorted rebar created significant bending effects in the tensile tests. Although this effect is small, when combined with other flaws, the distortion of the rebar could

cause premature failure. The inconsistent outer wrap initiated failure due to the already high strain levels at this critical location.

Of the two kinds of E-glass bars tested, both were at least 45% fiber volume in a polyester or vinylester matrix. The difference in the bars was primarily in their outer surfaces; one had an outer layer of matrix material for protection while the other had a sanded exterior with protruding deformations. The exterior one-eight-inch outer coatings on the rebar are used to increase fiber protection and, in the case of the protruding deformations, improve the pullout characteristics from concrete. These bars underwent three test series. In these tests, the specimens had a diameter of approximately 0.75 inches and were 42 inches long with a large clear spacing between grips where two linear voltage displacement transducer(LVDT) with a gauge length of 12 inches were attached. The first series of tests served as a baseline. These tests followed ASTM D3916. The next series of tests used a clamp grip tightened directly onto the rebar. The final test used a clamp grip and the rebar was further protected by a wrapping the ends with additional composite material. A substantial increase in the measured strength was found by using both the clamp and the end wrap. In this configuration, unlike the others, the failure was outside the grip, along the entire rebar, and the measured strength was expected to be the highest attainable for these bars, as reported in Table 2.1 [Malvar, Bish, 1995].

Table 2.1. Effect of Grip Type on Measured Mechanical Properties

Bar Type	Grip Type	Tests	Modulus of Elasticity GPa (ksi)	Ultimate Stress MPa (ksi)	Ultimate Strain
A	ASTM D3916	5	46.5 (6740) ± 1.3%	598 (86.7) ± 2.2%	0.0141 ± 3.4%
A	Clamp	3	---	617 (89.5) ± 2.7%	---
A	Clamp + Wrap 1	4	49.3 (7155) ± 9.0%	680 (98.6) ± 6.7%	0.0153 ± 4.0%
A	Clamp + Wrap 2	4	47.8 (6930) ± 6.6%	648 (93.9) ± 3.2%	0.0157 ± 9.1%
C	ASTM D3916	5	47.4 (6880) ± 2.4%	561 (81.4) ± 5.1%	0.0123 ± 6.5%
C	Clamp	3	---	710 (103.0) ± 5.1%	---
C	Clamp + Wrap 2	3	50.4 (7315) ± 3.0%	768 (111.3) ± 5.1%	0.0186 ± 21.2%

An extensive investigation on how resin properties affect impact strength was reported by Palmer [1981]. The same fiber, Thornel 300, together with 23 different resins, was used in the investigation. Longitudinal tensile strengths and strains to

failure are given for the different unidirectional systems in the report. It was shown that the composite strength increases with resin modulus. A closer examination shows that the increase is greater than what can be expected from the rule of mixtures and the strengthening must be caused by an interaction between fiber and matrix. The data have been used to plot the composite strength versus resin strain to failure in Figure 2.11 and composite strain to failure versus resin strain to failure in Figure 2.12. These two graphs show that the composite strength and strain to failure increases with matrix strain to failure. It can be expected that a matrix with a higher strain to failure has a higher toughness than a matrix with a lower strain to failure. Sufficient data for strength modeling with the clustering models as given in Section 3 are not available. However, the models predict that the critical defect size increases with matrix toughness and this would cause an increase in composite strength as seen in this study.

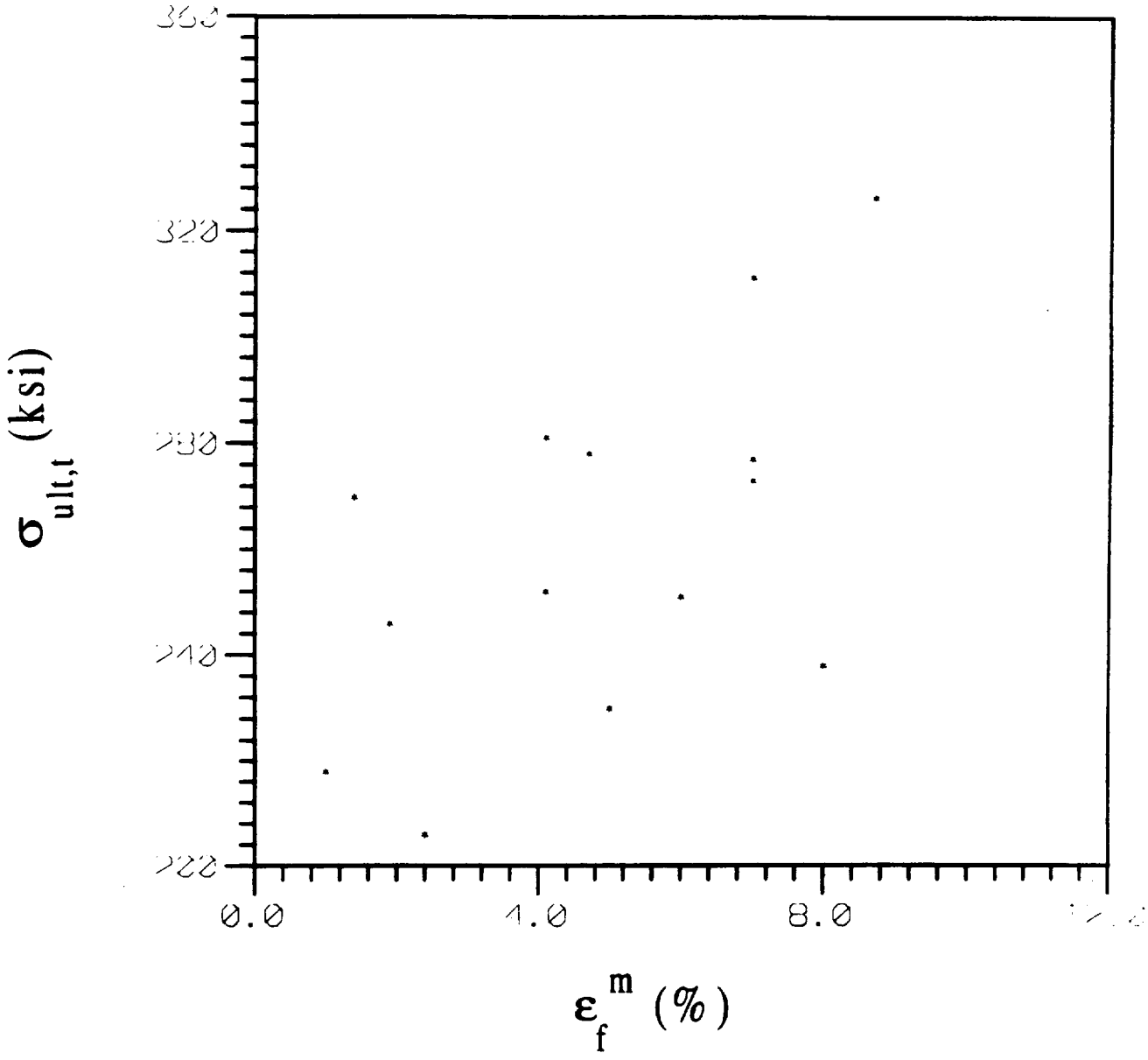

Figure 2.11. Composite strength to failure as a function of resin strain.

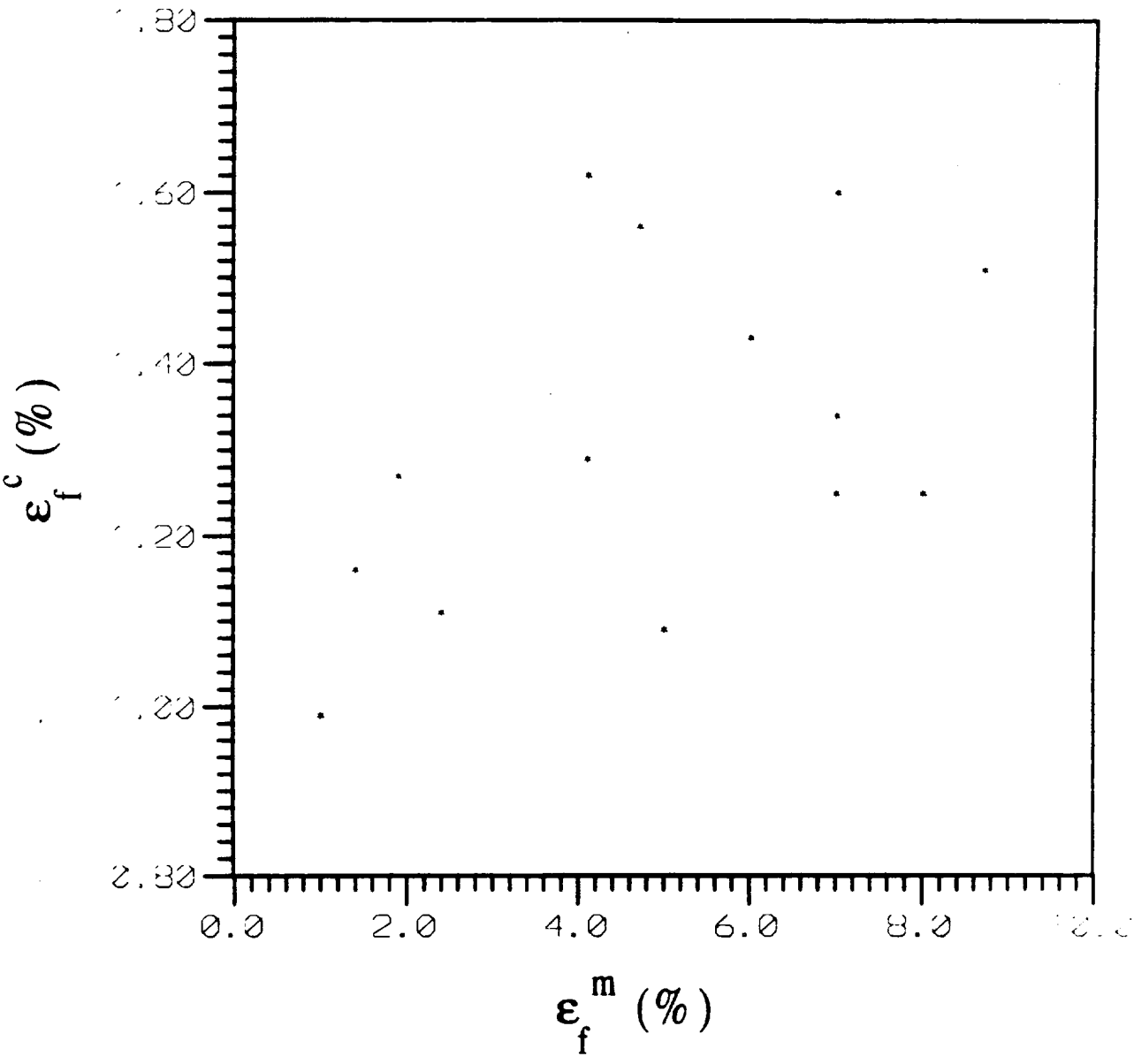

Figure 2.12. Composite strain to failure as a function of resin strain.

3.0 THEORETICAL DEVELOPMENT OF STRENGTH AND DUCTILITY

This section describes analytical models that have been developed to assess the strength and ductility of unidirectional composites. Many large components made of composite materials do not exhibit the strength expected of specimen data that is especially critical for large civil structures. This can be attributed to a volume dependence of the composite material's strength, introduction of unknown defects during the manufacturing of larger complex components, unexpected residual stresses, or stress concentrations. A volume dependence of the tensile strength has been observed for PMCs. Bullock [1974] found that this variation could be represented by a two-parameter distribution (Weibull [1939]). Later, it was observed by Whitney and Knight [1980], who had access to more experimental data, that the two-parameter distribution was not sufficient to model the strength. For a brittle-brittle composite system, Jansson and Leckie [1992] observed a substantial difference between the tensile and bending strengths for different flexural modes. This large difference in strength was attributed to the formation of a macroscopic defect requiring a number of clustered fiber breaks.

The fiber strength is frequently represented by a two-parameter Weibull distribution that is based on the weakest link assumption. Unidirectional fiber-reinforced composites usually exhibit a lower volume dependence in strength than the individual fibers. In this type of composite, the fibers are parallel and the weakest link

concept for the individual fibers is not likely to apply because a break in an individual fiber causes a stress redistribution and the load is carried by the remaining unbroken fibers. This feature was addressed in the analysis of a dry fiber bundle by Daniels [1945]. For a large bundle, many fibers are engaged in the failure and the strength is deterministic with an effective bundle length that is equal to the length of the composite. The concept of a fiber bundle was later modified to include the contribution to the load-carrying capacity from sliding between matrix and broken fibers, cf., Sutcu [1989], Thouless and Evans [1988] and Curtin [1993]. The load transfer to the surrounding matrix causes the effective fiber bundle length to be shorter than the gauge length and has been related to the stress recovery length of a broken fiber, cf., Phoenix [1993], Curtin [1993] and Jansson and Kedward [1996]. This type of failure, where the load carried by a broken fiber is redistributed equally between the still-intact fibers, is commonly denoted as global load sharing.

Another extreme of behavior was suggested by Zweben and Rosen [1970]. In their model, it is assumed that a critical defect is formed when a secondary break adjacent to a previously broken fiber occurs and the load-carrying capacity of the composite is lost. This leads to a Weibull modulus for the composite that is approximately twice the value of the fiber modulus. This type of failure is denoted as local load sharing.

Coleman [1958] showed that a fiber bundle with a finite number of fibers has a variability in strength. This variability decreases as the number of fibers in the bundle increases. This variation in the strength of finite fiber bundles was used by Gücer and

Gurland [1962]. They assumed that the composite consists of layers in series and each layer consists of a number of fiber bundles. A layer loses its load-carrying capacity when one bundle in the layer breaks and a weakest-link system is formed in the layers of the composite material. These models have been refined and references are given in Phoenix [1993]. The actual size of the fiber bundle is frequently determined by fitting the model to composite strenth data. This implies that such models cannot be used to study how the matrix and interface influences the composite strength.

In this section, a simple model for a composite that exhibits perfect fiber fragmentation is presented. It is shown that the strength and ductility predictions for this model compare favorably to other expressions available in the literature, such as when compared to a detailed numerical analysis of the same problem by Neumeister [1993]. This type of fragmentation model gives an indication of the achievable strength and ductility for a composite. However, many composites fail before the fragmentation strength is reached. This is caused by the clustering of fiber breaks into a large defect that triggers a global failure. The fragmentation model is used together with a statistical model for the clustering of fiber breaks to determine the strength for different composite systems. Some new aspects of the local load-sharing model are also discussed in relation to clustering of fiber breaks.

3.1 Model for Fiber Fragmentation

Consider the unidirectional composite that is depicted in Figure 3.1. Following Jansson and Kedward [1996],a the average stress in the longitudinal direction is given as

$$\bar{\sigma}_1 = f\sigma_1^f + (1-f)\bar{\sigma}_1^m \tag{3.1}$$

where f is the fiber volume fraction and the average stresses for the two phases are given by

$$\bar{\sigma}_1^{\alpha} = \frac{1}{v_\alpha}\int_{v_\alpha}\sigma_1^{\alpha}\,dv \tag{3.2}$$

where v_α is the volume of each phase. Assume that the composite is subjected to a strain field with an average strain $\bar{\varepsilon}_1$ in the longitudinal direction. Furthermore, the strain field is such that no average transverse stresses develop. For a composite with a brittle matrix, cracking occurs transverse to the fiber direction before the ultimate strength is reached, causing $\bar{\sigma}_1^m = 0$ at failure. In the case of a PMC, the matrix contribution to the longitudinal stress could be considered to be insignificant because of the relatively low stiffness of the matrix. For an MMC with a ductile matrix, the matrix can carry a significant load and the phase average can, to a good approximation, be assumed to be given by the uniaxial stress-strain relation for the matrix as

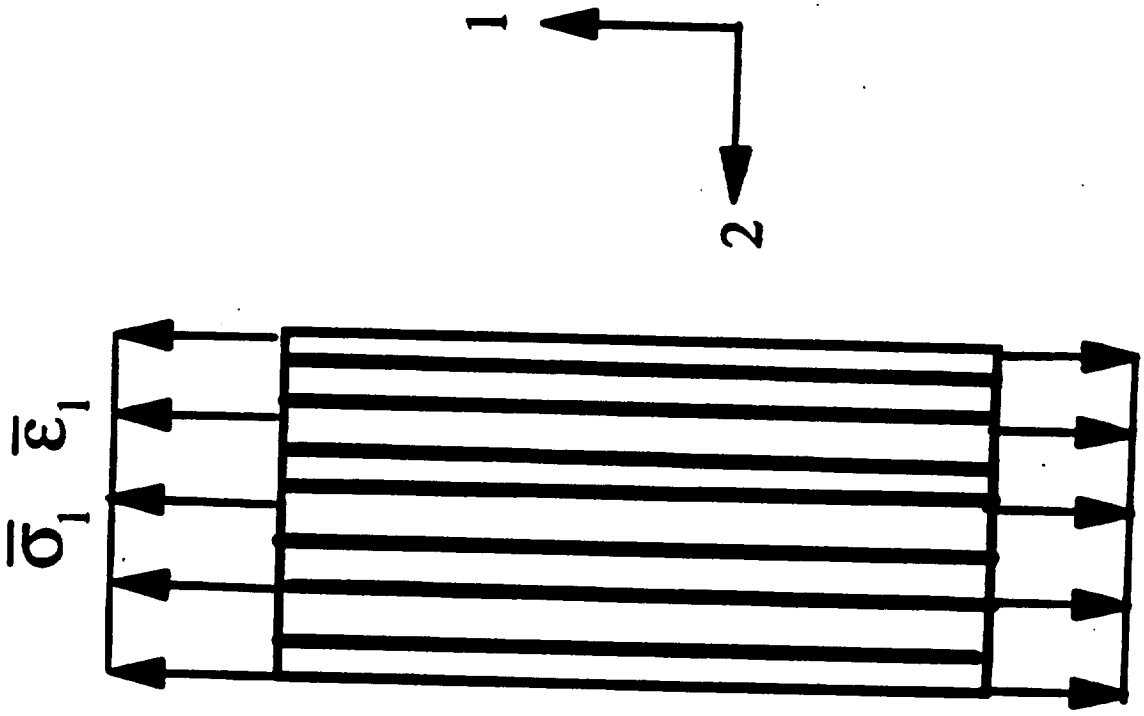

Figure 3.1. Example of an unidirectional composite.

$$\bar{\sigma}_1^m = \sigma^m(\bar{\varepsilon}_1) \tag{3.3}$$

The strength of brittle fibers is often expressed in statistical terms. For a simple two-parameter Weibull distribution [Weibull, 1939], the survival probability for a single fiber of length l is given as

$$P_s = \exp\left(-\frac{l}{l_0}\left[\frac{\sigma^f}{\sigma_0}\right]^m\right) \tag{3.4}$$

where σ^f is the stress in the fiber, l_0, σ_0 and m are constants governing the strength distribution of the fiber. A high value of the Weibull modulus, m, indicates a low variability in strength. If a single fiber could be subjected to a stress σ^f throughout the whole length, then the number of breaks in the fiber would be

$$n = \frac{l}{l_0}\left[\frac{\sigma^f}{\sigma_0}\right]^m \tag{3.5}$$

For a fragmented fiber in a composite with a surrounding matrix, stress recovery occurs at the fiber breaks and the stress gradually builds away from the break to the far field value. This causes the number of actual breaks for a fiber in a composite to be lower than what is given by Equation 3.5. Assuming that the breaks are well separated and that the linear stress recovery model by Kelly and Tyson [1965] applies,

the stress distribution given in Figure 3.2 would be present in a fiber. The recovery length is given as

$$l_R = \frac{d\sigma^f}{4\tau_s} \tag{3.6}$$

where τ_s is a constant sliding resistance at the fiber matrix interface and d is the fiber diameter. In reality, the stress recovery is quite complex with a sliding zone and an elastic recovery region. Experimental data are frequently evaluated in terms of this simple model and the reported sliding resistance only represents an average value in a simplified model of stress recovery. Differentiation of Equation 3.5 with respect to stress gives

$$dn = \frac{lm(\sigma^f)^{m-1}}{l_0(\sigma_0)^m} d\sigma^f \tag{3.7}$$

For the fiber stress distribution given in Figure 3.2, new breaks can only occur in the regions of the fibers that can be subjected to a stress increase, which are given by portions of the fiber that have a constant stress distribution. Hence, the effective length in which new fiber breaks can occur is

$$l = L - 2nl_R \tag{3.8}$$

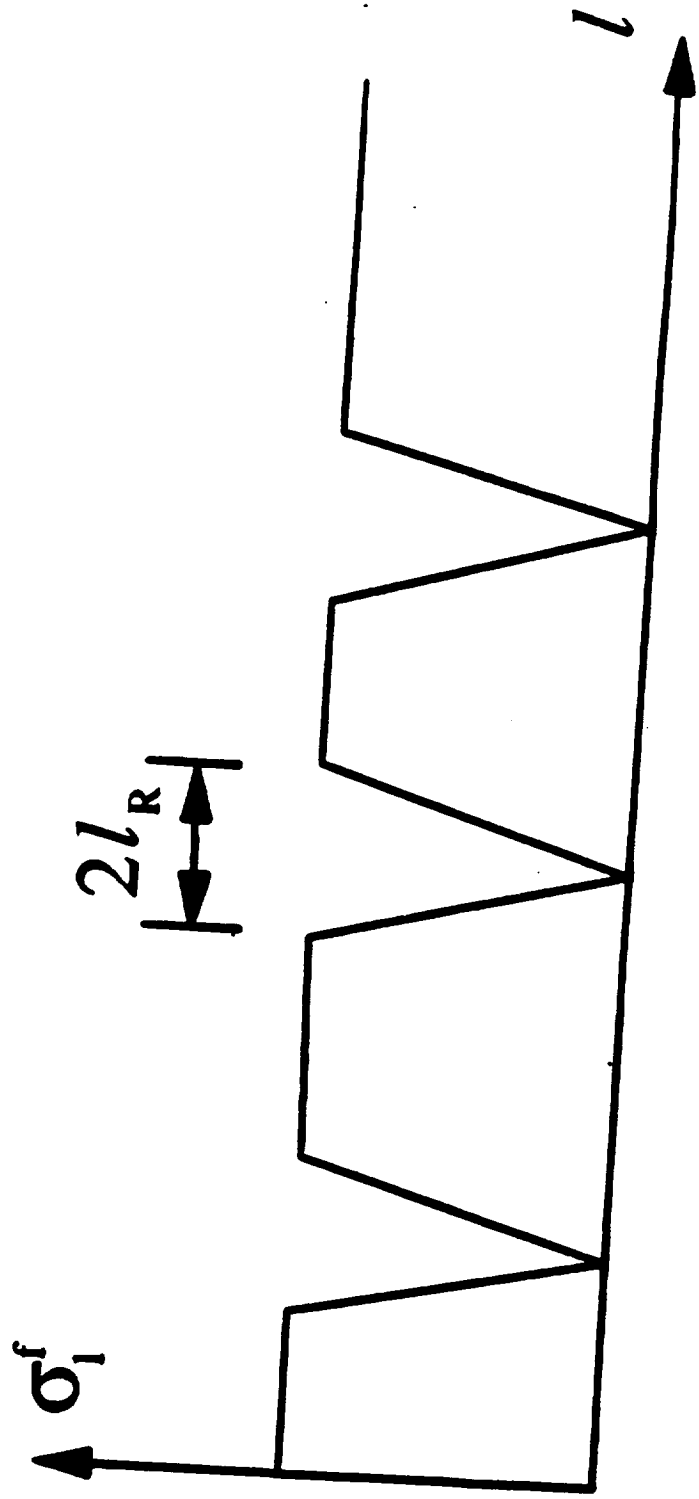

Figure3.2. Stress distribution in fragmented fibers.

where L is the total fiber length in the composite. Use of this relation in Equation 3.7 gives

$$dn = \frac{(L - 2nl_R)m(\sigma^f)^{m-1}}{l_0(\sigma_0)^m} d\sigma^f \tag{3.9}$$

This equation can be integrated and expressed in an integral form when l_R depends on stress. However, for simplicity, assume that l_R is independent of stress during the integration. This assumption gives

$$n = \frac{L}{2l_R}\left[1 - \exp\left(-\left[\frac{\sigma^f}{\sigma_R}\right]^{m+1}\right)\right] \tag{3.10}$$

where

$$_R = \left(\frac{2l_0\tau\sigma_0^m}{d}\right)^{\frac{1}{m+1}} \tag{3.11}$$

The average stress in the fiber phase of the composite can be determined from the fiber stress distribution given in Figure 3.2. Applying Equation 3.2 and integrating over the total length L of all the fibers gives

$$\bar{\sigma}^f = \frac{1}{L}\int_0^L \sigma^f(x)dx = \sigma^f\left[1 - \frac{nl_R}{L}\right] \tag{3.12}$$

Using Equations 3.10 and 3.6 in 3.12 gives finally

$$\bar{\sigma}^f = \frac{\sigma^f}{2}\left[1 + \exp\left(-\left[\frac{\sigma^f}{\sigma_R}\right]^{m+1}\right)\right] \tag{3.13}$$

where

$$\sigma^f = E_f\bar{\varepsilon} \tag{3.14}$$

This equation constitutes an uniaxial stress-strain relation for the fiber portion of the composite, while the full stress-strain relation for the composite is given by Equation 3.1. The stress-strain relation given by Equation 3.13 is shown in normalized form in Figure 3.3 for m equal to 8. It can be deduced that first the stress increases monotonically with strain until a local load maximum is reached. Thereafter, the stress decreases and finally begins to slowly increase again with strain. The model's accuracy is diminished after the load maximum is reached and should only be used with confidence up to the load maximum. When the local load maximum is reached, a localization occurs because the stress level decreases with strain after this point. Hence, the local load maximum dictates the ultimate strength and is given by the condition

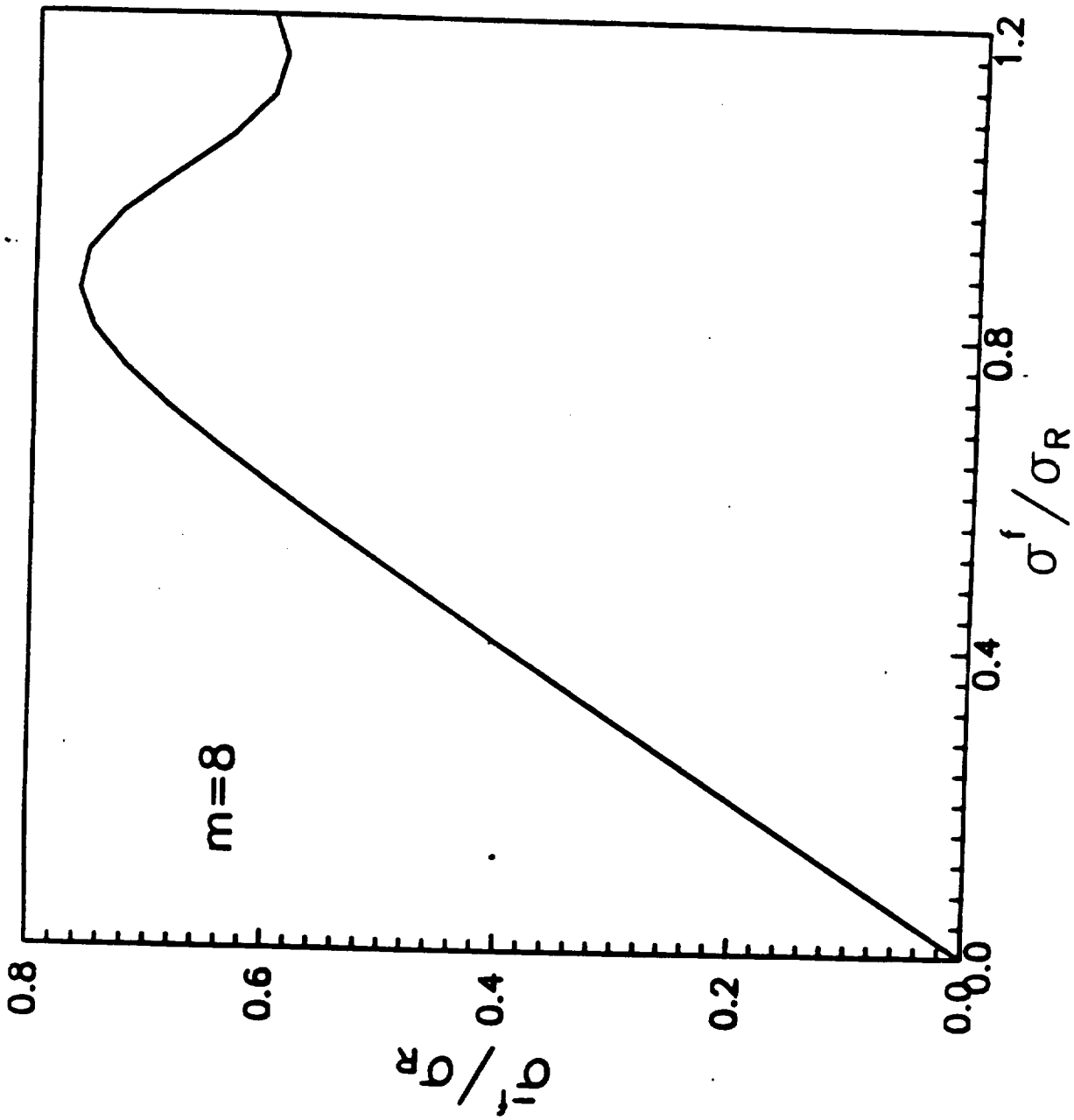

Figure 3.3. Normalized stress-strain relation for the composite as given by Equation 3.13.

$$\frac{\partial \bar{\sigma}^f}{\partial \sigma^f} = 0 \tag{3.15a}$$

because of the linearity of Equation 3.14. Applying Equation 3.15a in Equation 3.13 gives

$$+\exp\left[-\left(\frac{\sigma^f}{\sigma_R}\right)^{m+1}\right]\left[1-(m+1)\left(\frac{\sigma^f}{\sigma_R}\right)^{m+1}\right] = 0 \tag{3.15b}$$

A numerical evaluation of this expression shows that m must be greater than 2.7 for the model to have a load maximum. A straightforward linearization of Equations 3.15b and 3.13 gives the ultimate strength as

$$\bar{\sigma}_M^f = \sigma_R\left[\frac{2}{(m+2)}\right]^{\frac{1}{m+1}}\frac{m+1}{m+2} \tag{3.16}$$

which is exactly the same result as derived by Curtin [1993]. A more accurate result can be obtained by seeking the solution for the load maximum in the following form

$$\left.\frac{\sigma^f}{\sigma_R}\right]^{m+1} = \frac{\beta}{m} \tag{3.17}$$

where β has to be determined. Inserting Equation 3.17 into Equation 3.15b and collecting terms of different order in 1/m gives

$$0 = (2-\beta) + \frac{\beta(\beta-2)}{m} - \frac{\beta^2(\beta-3)}{2m^2} + \frac{\beta^3(\beta-4)}{2m^3} \ldots\ldots \tag{3.18}$$

By choosing β equal to 2, the condition for the load maximum is satisfied by the two leading terms of the series expansion and is also asymptotically correct for large values of m. Use of this result in Equation 3.13 gives the following expression for the load maximum

$$\bar{\sigma}_M^f = \frac{\sigma_R}{2}\left(\frac{2}{m}\right)^{\frac{1}{m+1}}\left[1+\exp\left(-\frac{2}{m}\right)\right] \tag{3.19}$$

The strength predictions for this model are compared with the numerical solution by Neumeister [1993] in Figure 3.4. This model also compares favorably with the detailed numerical simulation of the expressions given by Curtin, [1993] and Phoenix [1993] and can be used with confidence in the subsequent strength models.

One aspect that has been overlooked in the discussions of composite strength is the strain at which the load maximum occurs. The composite average strain is related to the fiber stress far away from the break by Equation 3.14. The average strain at the load maximum can thus be determined by using this relation and inserting the fiber stress at the load maximum in Equation 3.14, to give

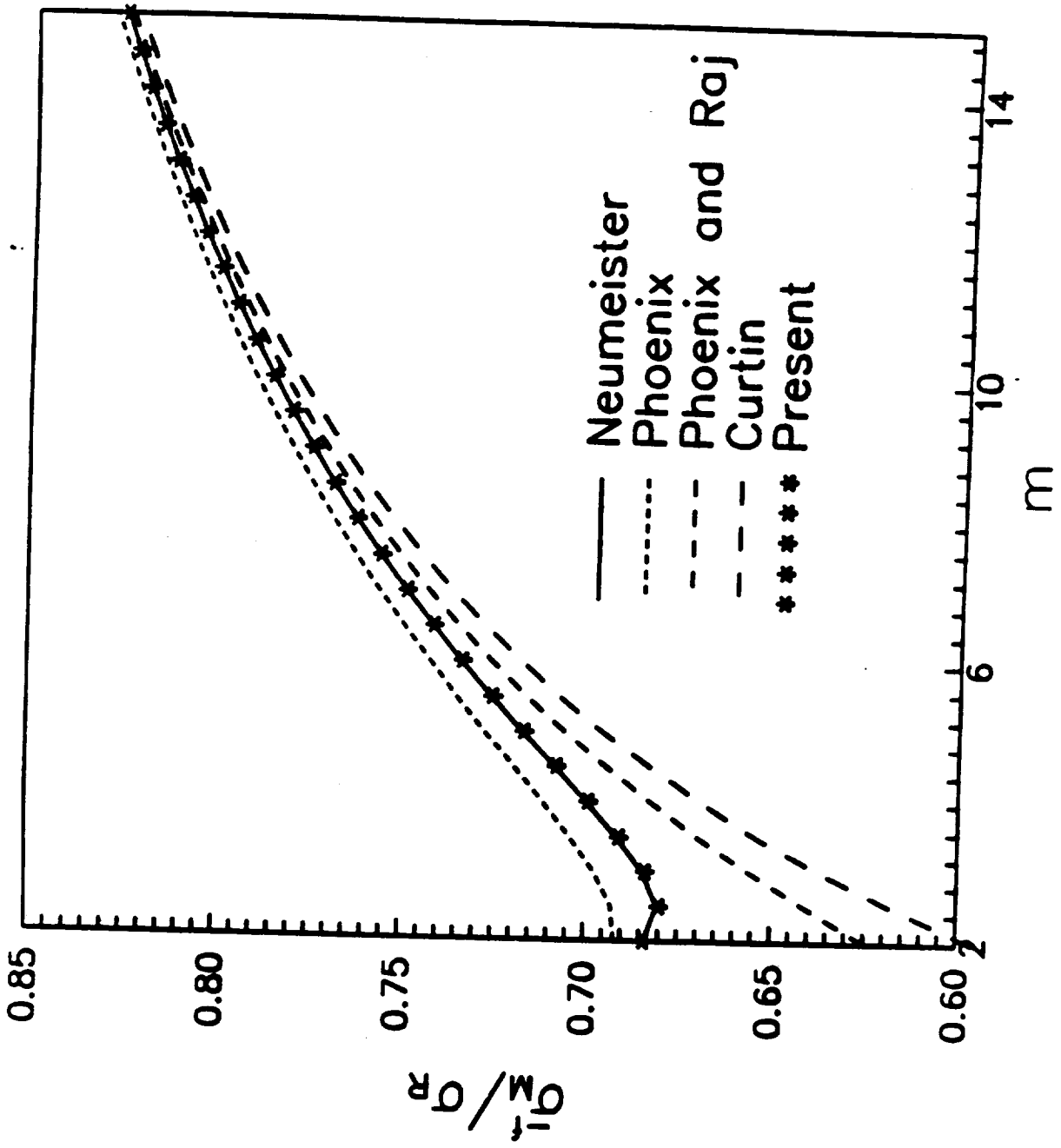

Figure 3.4. Normalized strength predictions for the current model compared with other numerical simulations.

$$\bar{\varepsilon} = \frac{\sigma_R}{E_f}\left(\frac{2}{m}\right)^{\frac{1}{m+1}} \tag{3.20}$$

The strain at the load maximum is shown in normalized form in Figure 3.5 together with the numerical simulations by Neumeister [1993] and the other models. It can be concluded that all the closed-form solutions underestimate the strain at the load maximum. Of these examples, the present model has the lowest discrepancy. The lower strain prediction occurs because the possibility of an overlap of the slip regions has been ignored in this model.

The model given by Equation 3.14 is equivalent to the assumption that the load-carrying capacity of the composite is given by a fiber bundle of length $2l_R$ which has a frictional sliding contribution from the pullout of the broken fibers with an effective sliding length of $l_R/2$.

This type of fiber-fragmentation model should be viewed as an indicator of the maximum achievable, longitudinal strength and strain at the load maximum of a composite. Many different failure events can occur before this strength is reached. Some of these failures will be discussed in subsequent paragraphs.

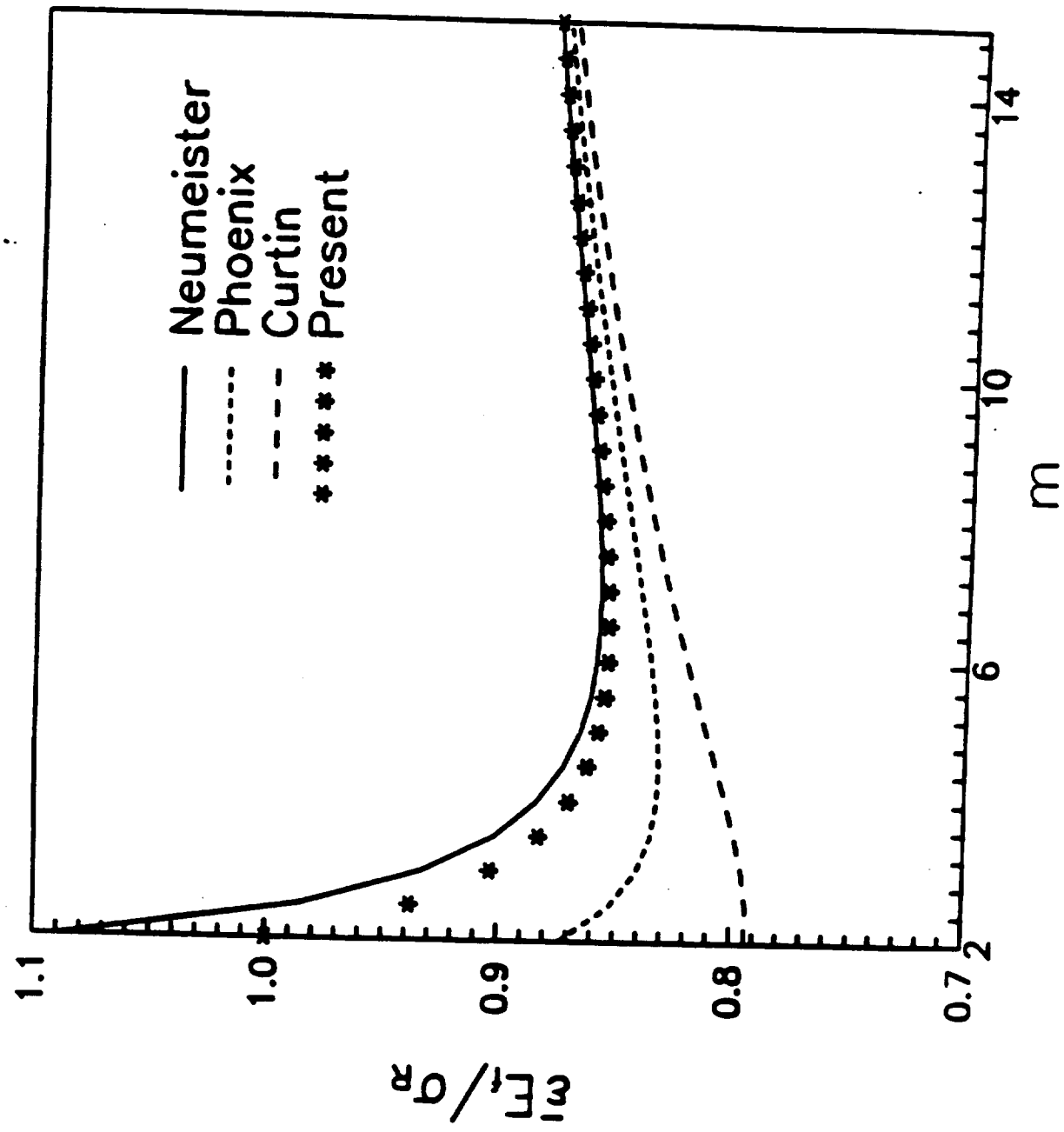

Figure 3.5. Normalized strain at the load maximum compared with other numerical simulations.

3.2 Failure by a Mode I Crack

A global failure of a composite occurs when a macroscopic defect is formed. This defect can be characterized as one of a number of different global failure types which can occur in a composite before the perfect fragmentation strength is reached. For some composites, experiments indicate that the fracture planes are perpendicular to the fibers and the loading direction. This suggests that the macroscopic failure for the present composite is given by the formation of a mode I crack [Bish, Jansson and Kedward, 1996]. It will be assumed that the critical crack is formed when a sufficiently large local fiber bundle has reached its load maximum. The crack opening is then exerted on by the fiber portion of the composite stress and the matrix still bridges the crack because of its higher ductility. The diameter of the fiber bundle that fails has to be sufficiently large in order to be able to drive the growth of defects. For linear elastic fracture mechanics, the radius of the bundle is related to the toughness as

$$a = \frac{1}{\pi}\left(\frac{k_{IC}}{f\sigma_f}\right)^2 \tag{3.21}$$

where it has been assumed that the broken fibers cause an opening of the crack while the matrix still bridges the crack. It is further assumed that only fiber breaks within one transfer length, l_T, from the crack face affect the opening mode of the crack. This implies that the volume of the critical defect, or the local fiber bundle is

$$v_h = 2l_R\pi a^2 = \frac{dk_{IC}^4}{2\pi f^4 \tau \sigma_f^3} \qquad (3.22a,b)$$

The total length of fibers in this volume is given by the relation

$$l_{hf}\frac{\pi d^2}{4} = f 2\pi a^2 l_R \qquad (3.23)$$

The average number of fiber breaks in one bundle can the be determined by use of $L = l_{hf}$ and Equations 3.11 and 3.23 in Equation 3.10 gives

$$n = \frac{L}{2l_R}\left[1 - \exp\left(-\frac{d\sigma_f^{m+1}}{2l_0\sigma_0^m\tau}\right)\right] \qquad (3.24)$$

and the number of breaks at the load maximum is

$$\bar{n} = \frac{2L\tau}{d}\left(\frac{md}{4l_0\sigma_0^m\tau}\right)^{\frac{1}{m+1}}\left[1 - \exp\left(-\frac{2}{m}\right)\right] \qquad (3.25)$$

Because of the statistical nature of the fiber breaks, the breaks will cluster in some regions. This is a well-known phenomenon in statistics and the probability of finding $\bar{n}$ breaks inside v_h, when the average numbers of breaks in v_h is n, is given by a Poisson distribution as

$$p(n=\bar{n}) = e^{-n}\frac{n^{n}}{\bar{n}!} \tag{3.26}$$

The fiber bundle is at the load maximum when this value is reached. However, it will also have reached the load maximum if more breaks have occurred. This condition is given by the cumulative Poisson distribution as

$$p(s \geq \bar{n}) = \frac{\gamma(\bar{n}, n)}{\Gamma(\bar{n})} \tag{3.27}$$

where γ is the incomplete and Γ is the complete gamma function. Hence, the probability that a fiber bundle has reached the load maximum and a critical defect is formed, is given by this expression. This can occur at any location in the composite and the survival probability of the composite can then be determined by using a weakest-link approximation for the composite as

$$p_s = \prod (1 - p_f') \approx \exp\left(-\int_v \frac{\gamma(\bar{n}, n)}{\Gamma(\bar{n})}\frac{dv}{v_b}\right) \tag{3.28a, b}$$

where n is given by Equation 3.24, $\bar{n}$ by Equation 3.25 and v_b by Equation 3.22. The result, Equation 3.28b is based on the assumption that $p_f' <<$, which is usually the case.

This strength model was used by crack [Bish, Jansson and Kedward, 1996] to model the strength for a unidirectional MMC composite. It was found that traditional Weibull statistics could not predict the strength for different specimen volumes and loading modes. As can be seen in Table 3.1, this model predicts with a high level of accuracy observed differences in strength.

Table 3.1. Experimental and Theoretical Strength Factors for SCS6/Ti 15-3

Type	Experimental Strength Factor	Theoretical Strength Factor Linear Stress Distribution	Non Linear Stress Distribution
Short Tension	1	1	1
Long Tension	0.97	0.95	0.96
4-Pt Bending	1.28	1.19	1.22
Long 3-Pt Bending	1.37	1.45	1.39
Short 3-Pt Bending	1.40	1.68	1.5

3.3 Failure by Bundle Pullout

Some systems have a weak, brittle matrix and the global failure is caused by uninhibited shear crack propagation in the longitudinal direction [Neumeister et al, 1996]. This type of cracking will allow weak regions at different locations in the composite to link up, forming a global failure. Hence, the strength is given by the formation of a mode II crack that in turn is caused by a bundle pullout mechanism. The failure is anticipated when an element, as shown in Figure 3.6, with diameter D_B and length L_R, fails. It is assumed that local interaction in the longitudinal direction is limited to one stress recovery length, L_R. The diameter, D_B, of the smallest bundle

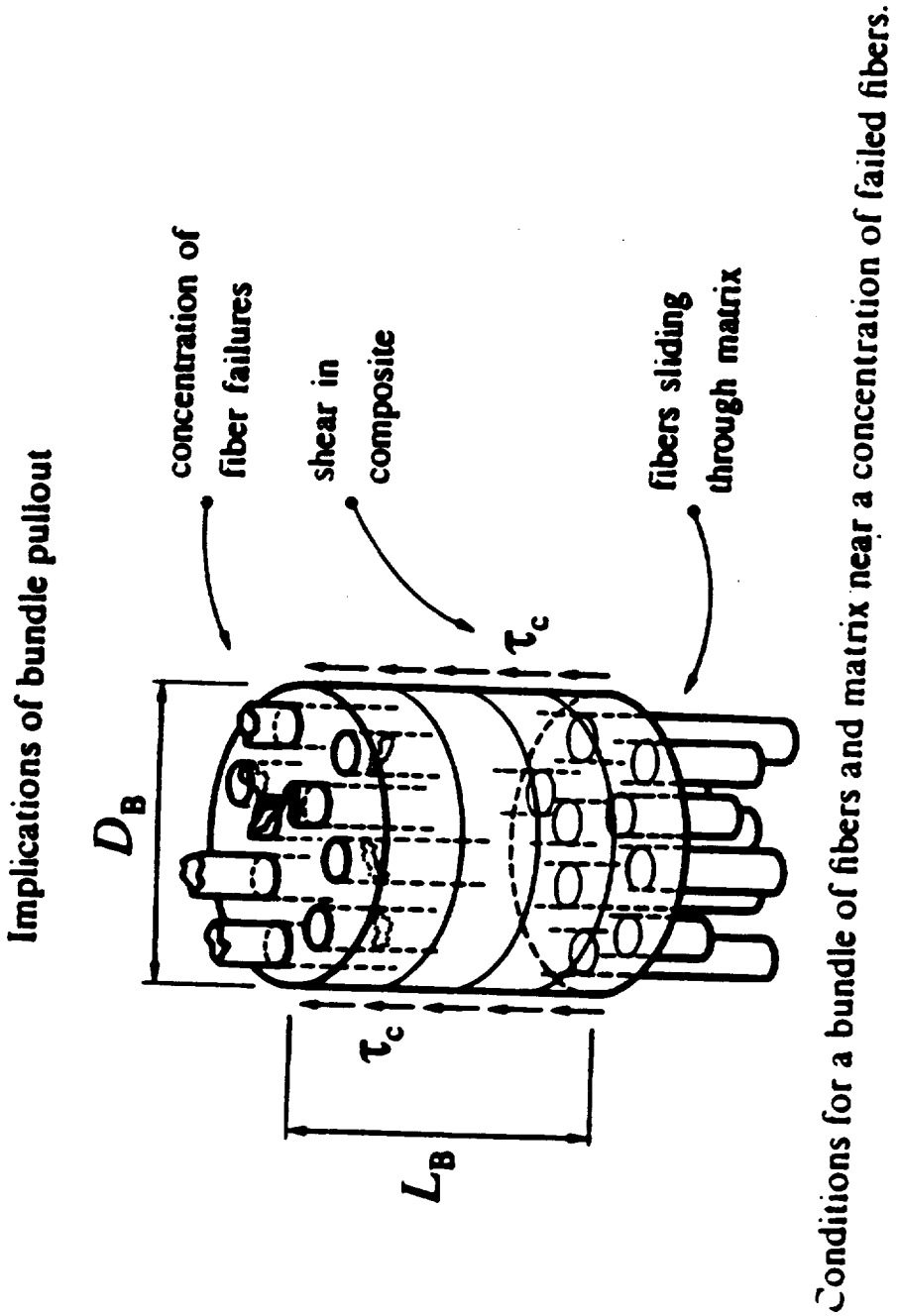

Figure 3.6. Conditions for a bundle of fibers and matrix near a concentration of failed fibers.

element that can be pulled out is given by a balance of the interlaminar shear strength τ_c and interfacial sliding stress τ_i as

$$\pi D_B L_R \tau_c = n_B \pi d L_B \tau_i \tag{3.29}$$

The use of this definition of the fiber volume fraction and Equation 3.6 give the element volume as

$$V_B = \frac{\pi d^3 \tau_c^2 E_f \sigma_f}{16 f^2 \tau_i^3} \tag{3.30}$$

The number of breaks in the fiber bundle can be determined by use of Equations 3.10 and 3.11 as

$$n = \frac{1}{2_f}\left(\frac{\tau_c}{\tau_i}\right)^2\left[1 - \exp\left(-\frac{d\sigma_f^{m+1}}{2l_0\sigma_0^m\tau}\right)\right] \tag{3.31}$$

and the number of breaks at the load maximum is given by

$$\bar{n} = \frac{1}{2f}\left(\frac{\tau_c}{\tau_i}\right)^2\left[1 - \exp\left(-\frac{2}{m}\right)\right] \tag{3.32}$$

Failure is predicted when a critical fiber break density is reached within the element. An element becomes unstable when use of weakest-link statistics, as previously described, gives the survival probability as

$$p_s = \exp\left(-\int_v \frac{\gamma(\bar{n}, n)}{\Gamma(\bar{n})} \frac{dv}{v_B} \right) \tag{3.33}$$

Use of this model for the data for the Nicalon/LAS composite [Jansson and Leckie, 1994] is shown in Table 3.2. It can be deduced that this model predicts the strength ratios accurately for the different loading modes. Traditional Weibull statistics could not predict these differences.

Table 3. 2. Experimental and Theoretical Strength Factors for Nicalon/LAS

Type	Experimental Strength Factor	Theoretical Strength Factor
Tension	1	1
4-Pt Bending	1.33	1.25
3-Pt Bending Rectangular	1.49	1.33
3-Pt Bending Triangular	1.51	1.52

3.4 Local Load-Sharing Model

An improved analysis given for the local load-sharing model used by Zweben and Rosen [1970] is presented in this section. In this model, it is assumed that a critical defect is formed and failure of the composite occurs when a secondary break occurs in

a neighboring fiber to a previously broken fiber. The secondary break has to occur within one stress recovery length from the initially broken fiber. The initial fiber break causes a stress concentration, depicted in Figure 3.7, over a length $2l_R$ in the next neighboring fibers. The probability that the segment of length $2l_R$ of an adjacent fiber survives to the stress level σ_f experienced before the fiber break is

$$P_s^0 = \exp\left(-\frac{2l_R}{l_0}\left(\frac{\sigma_f}{\sigma_0}\right)^m\right) \tag{3.34}$$

and the probability that it survives the stress concentration caused by the fiber break is

$$P_s^1 = \exp\left(-\int_{-l_s}^{l_s}\left(\frac{\sigma_f(x)}{\sigma_0}\right)^m \frac{dx}{l_0}\right) = \exp\left(-\frac{2l_R\alpha k^m}{l_0}\left(\frac{\sigma_f}{\sigma_0}\right)^m\right) \tag{3.35}$$

where k is the highest stress concentration in the adjacent fibers and

$$\alpha = \frac{1-\frac{1}{k^{m+1}}}{(m+1)\left(1-\frac{1}{k}\right)} \tag{3.36}$$

for the present stress distribution as illustrated in Figure 3.7. For a constant stress distribution over the segment and $\alpha = 1$, the probability that an adjacent fiber survives

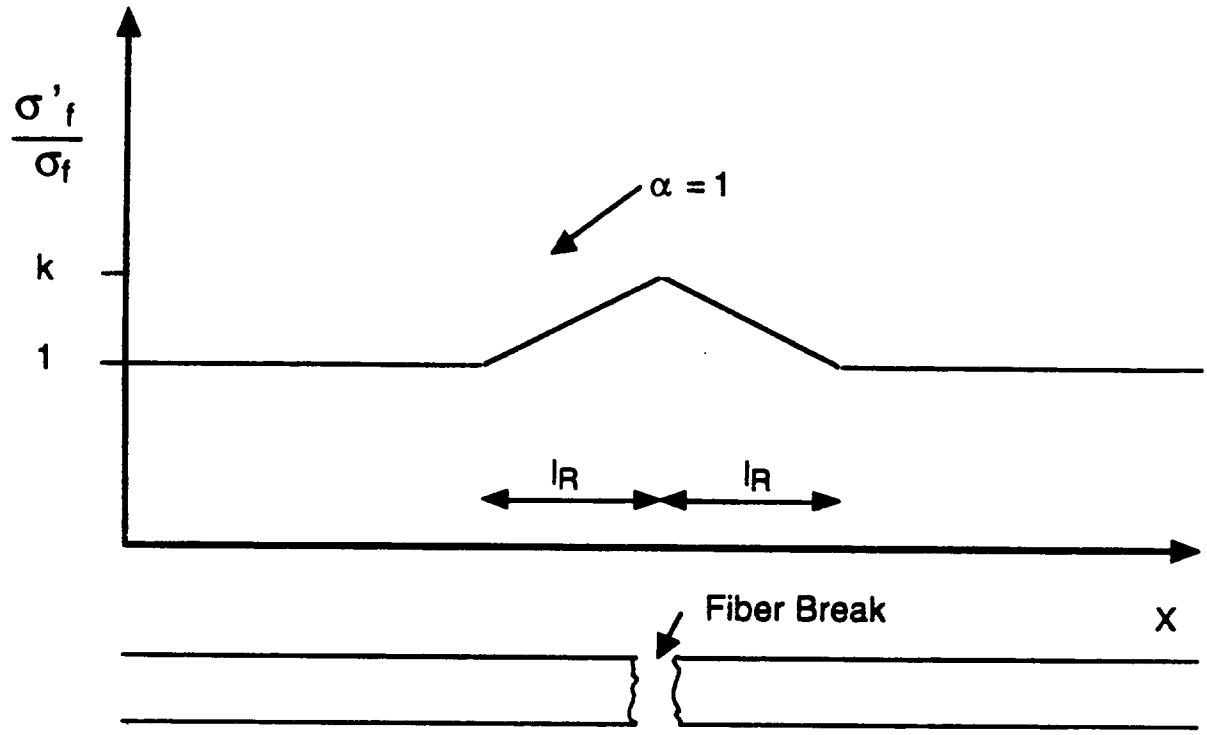

Figure 3.7. Stress distribution in fibers adjacent to a broken fiber.

to the stress level experienced before the initial break or breaks because of the stress concentration caused by the initial break is given by the conditional probability

$$P_f^2 = \frac{P_f^1 - P_f^0}{1 - P_f^0} \tag{3.37}$$

where $P_f^A = 1 - P_c^A$. The probability that all the β neighboring fibers survive is

$$P_c^3 = \left(1 - P_c^2\right)^\beta = \left(\frac{P_c^1}{P_c^0}\right)^\beta \tag{3.38}$$

The composite has n initial breaks that are given by Equation 3.10. Using a weakest-link assumption for the strength the survivor, probability for the composite is

$$P_c = \left(P_c^3\right)^n \tag{3.39}$$

Use of Equations 3.10 and 3.28b gives

$$P_c = \exp\left(-\frac{4f}{\pi}\frac{v}{l_0 d^2}[\alpha k^m - 1]\left(\frac{\sigma_f}{\sigma_0}\right)^m\left(1 - \exp\left(-\frac{d\sigma_f^{m+1}}{2l_0\sigma_0^m\tau}\right)\right)\right) \tag{3.40}$$

where v is the total volume of the composite. If

$$\frac{d\sigma_f^{m+1}}{2l_0\sigma_0^m\tau} << 1$$

then

$$P_s = \exp\left(-\frac{2f}{\pi}\frac{v}{l_0^2 d}[\alpha k^m - 1]\frac{\sigma_f^{2m+1}}{\sigma_0^{2m}\tau}\right) \tag{3.41}$$

For a globally varying stress distribution, the survival probability has to be integrated over the volume of the composite giving the relation

$$P_s = \exp\left(-\frac{2f}{\pi}[\alpha k^m - 1]\int_v \frac{\sigma_f^{2m+1}}{\sigma_0^{2m}\tau}\frac{dv}{l_0^2 d}\right) \tag{3.42}$$

This equation indicates that the Weibull modulus for the composite is 2m+1.

3.5 Failure by Clustering of Two Breaks

The critical defect in the local load-sharing model is given by two fiber breaks in adjacent fibers within two stress recovery lengths L_R. This failure can also be caused by clustering of two breaks. The probability of clustering of two breaks in adjacent fibers is given by Equation 3.28b by using

$$\bar{n} = 2 \tag{3.43}$$

and

$$L = 4l_R \tag{3.44}$$

The critical volume element is given by

$$v_0 = 2 \cdot 2l_R \frac{\pi d^2}{4} \frac{1}{f} = \frac{\pi d^3 \sigma_f}{4 f t} \tag{3.45}$$

to give

$$p_s = \exp\left(- \int_v \frac{\gamma(2,n)}{\Gamma(2)} \frac{dv}{v_0} \right) \tag{3.46}$$

A comparison between this model with global load sharing and other models which utilize the concept of local load sharing is shown in Figure 3.8. In the local-load sharing model, the redistribution of stress from a broken fiber is transferred only to the neighboring fibers. Thus, the stress concentration due to the failure of a fiber is confined to a localized area. An upper bound on the stress concentration is given by the assumption that the load from the broken fiber is carried only by the surrounding fibers, k is equal to 7/6. In reality, the load from the broken fiber is distributed over more fibers and the stress concentration is lower. A sliding fiber-matrix interface and matrix plasticity also reduce the stress concentration. A realistic number is $k = 1.07$. It can be deduced from Figure 3.8 that it is more likely that a composite will fail from clustering of two breaks than from the local stress concentration caused by a fiber break on the adjacent fibers.

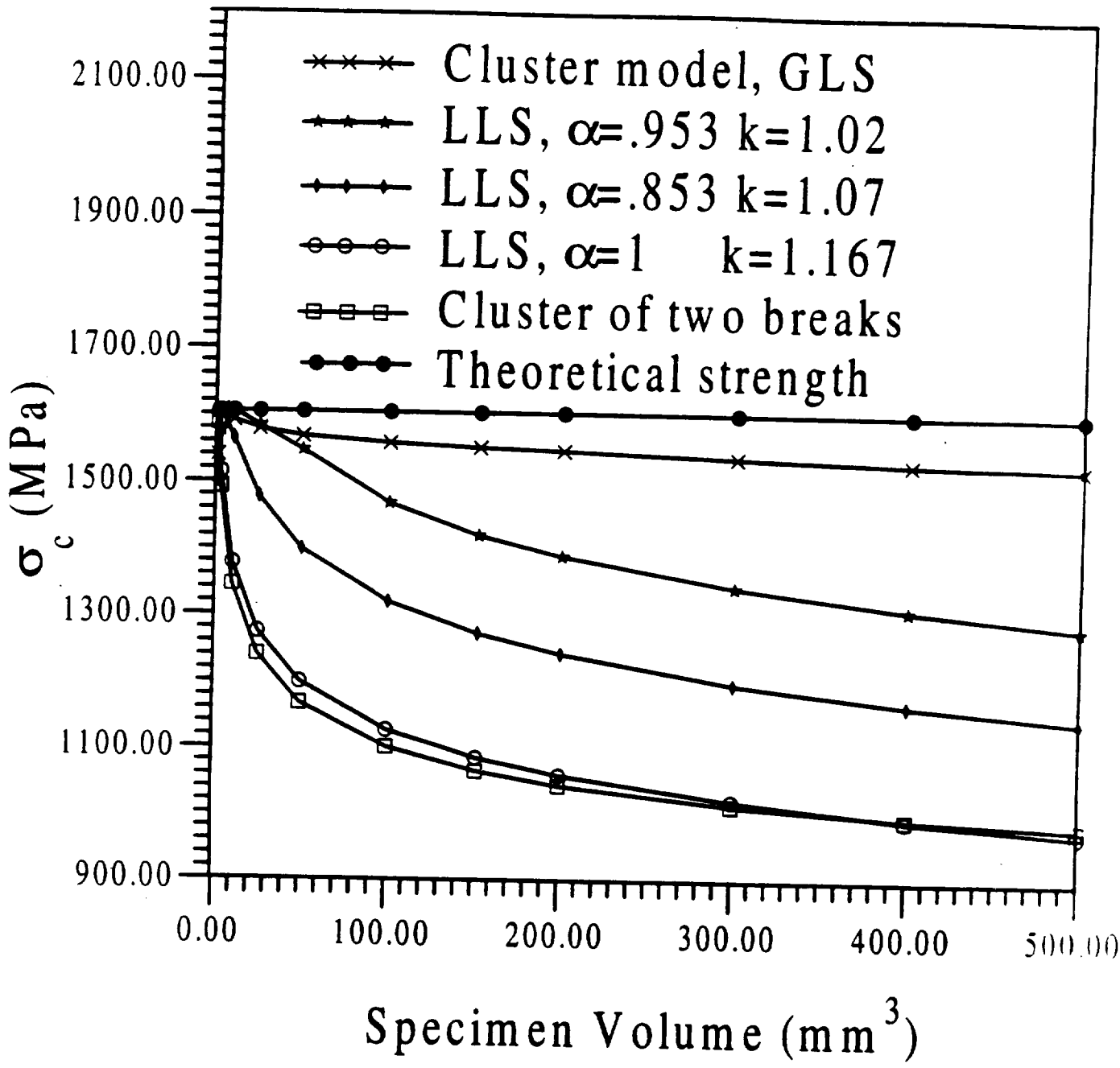

Figure 3.8. A comparison of models using the concepts of global and local load sharing.

4.0 STRESS REDISTRIBUTION IN COMPONENTS

Many components will be exposed to load and temperature variations for an extended time. The temperature and loading could be such that the stresses in the weaker and often softer phase of the composite, the matrix, relaxes. Some systems have a weak bond between fiber and matrix and this relaxation can dramatically change the matrix-dominated properties. Environmental effects, such a moisture, can also affect the bond between matrix and fiber in some systems. Here, some results are presented for an investigation on an MMC system for which the residual clamping pressure between fiber and matrix has been relaxed by subjecting the composite to a thermo-mechanical loading history.

4.1 Observed Mechanical Behavior.

4.1.1 Transverse Tension. The transverse tensile response is shown in Figure 4.1 for the pristine ($\varepsilon_1^c = 0$) and debonded composite ($\varepsilon_1^c = 0.5$) together with numerical simulations. It was found by Gunawardena et al., [1993] that the response of the pristine composite was modeled well by including the residual stresses from a fabrication temperature of 900°C and an interface that can only transfer compressive normal stresses and has a friction coefficient of $\mu = 0.8$. It is interesting to note that the initial linear response for the composite is slightly more compliant than that for a

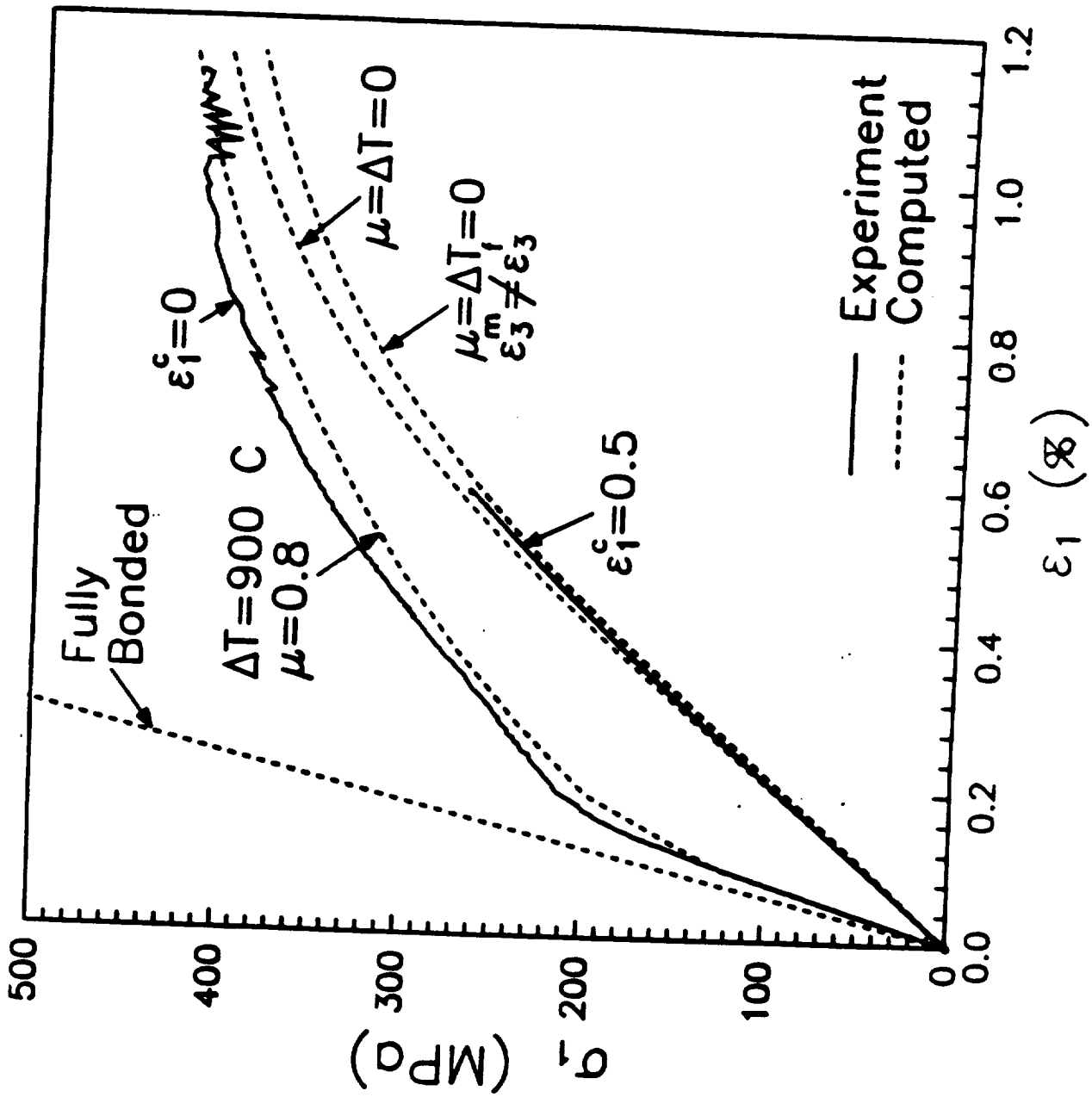

Figure 4.1. The transverse tensile response for the pristine ($\varepsilon_1^c = 0$) and debonded composite ($\varepsilon_1^c = 0.5$) together with numerical simulations.

composite with a fully bonded interface. After the initial linear response, a substantial decrease occurs in the slope of the stress-strain curve and this is caused by debonding at the fiber matrix interface. The computations also indicate that some localized yielding occurs in the matrix at the initial portion of the debond. Finally, the interface is fully debonded in the loading direction and the load-carrying capacity is dictated by the matrix ligaments between the fibers. A simple estimate for the transverse limit strength [Jansson et al, 1991] gives

$$\sigma_{TL} = \frac{2}{\sqrt{3}} A_{fm} \sigma_{l.m} \tag{4.1}$$

where A_{fm} is the matrix area fraction at the weakest plane and σ_{lm} is the limit strength of the matrix. The strain to failure is approximately 40% of the matrix failure strain of 3.2%. This reduction in failure strain is caused by a concentration of strain in the matrix ligaments between the fibers because they are subjected to a higher stress.

The response for the debonded composite, $\varepsilon_1^c = 0.5$, has a much more compliant initial linear response compared to the pristine composite. The modulus is only a third of the modulus for the pristine composite and is of the same magnitude as was observed for the same composite after cyclic thermo-mechanical load [Jansson et al., 1994]. It can be deduced that this response is modeled closely by assuming an initially stress-free interface, $\Delta T = 0$. The calculated response after debond is insensitive to the value of the coefficient of friction at the interface and quite insensitive to the constraint in the longitudinal direction. The response for the case where the fiber and

matrix have the same longitudinal strain is only slightly stiffer than the response for the case where the matrix is assumed to be fully decoupled from the fiber in the longitudinal direction, $\varepsilon_3^m \neq \varepsilon_3^f$.

The failure strain in the tensile test for the debonded composite is 0.6%. The specimen had previously accumulated a creep strain of 0.5%, giving a total strain of 1.1%. This total failure strain is very close to the observed failure strain for the pristine composite, indicating that a constant strain criteria could be used as a failure condition for this type of loading.

4.1.2 In Plane Shear. Shear tests have been performed with the fibers orientated in the direction of the two notches as shown in Figure 4.2. It was shown by Jansson et al. [1994] that the limit strength is dependent on the orientation of the fibers for composites with weak interfaces in this type of test. The present loading subjects a long portion along the fibers to constant conditions and is representative of loading that occurs in practical applications. It has a lower limit strength than the case where the fibers are oriented perpendicular to the notches. The experimental and computed stress-strain curves are shown in Figure 4.2.

The response for the pristine composite has a initial linear response followed by a gradual transition that reaches a limit condition with no increase in stress. A comparison with the numerical simulations indicated that no sliding occurs initially at the interface. This is followed by a response that corresponds to a sliding with a shear stress of 185 MPa at the interface. The sliding stress thereafter gradually decreases

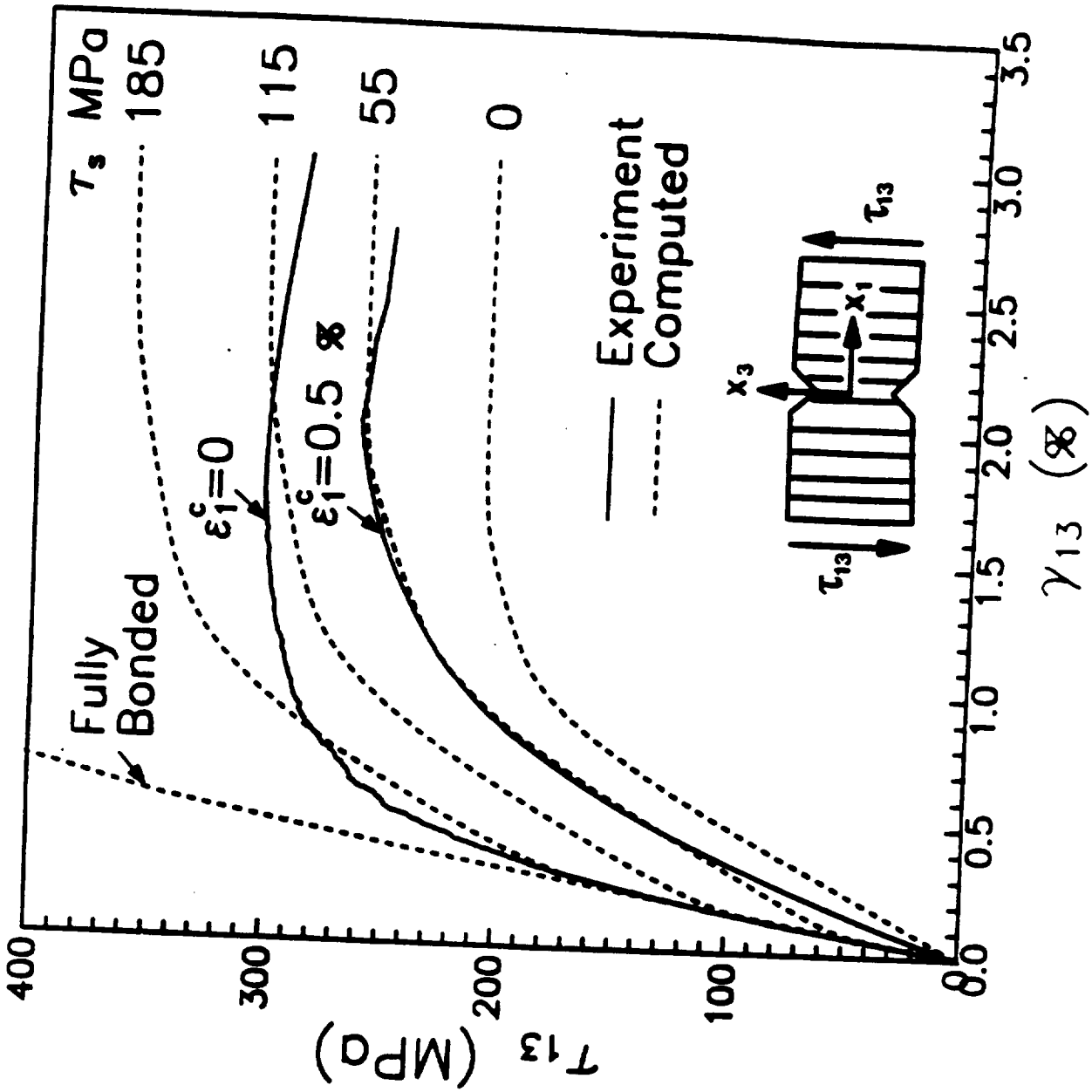

Figure 4.2. The experimental and computed stress-strain curves for in-plane shear loading conditions.

with increase in strain to a saturation value of 115 MPa. A simple model for the limit strength was proposed by Jansson et al., [1991]:

$$_{L} = \frac{1}{\sqrt{3}}\sigma_{l,m}A_{fm} + \tau_{y}^{'}\frac{\pi}{2} * (1 - A_{fm}) \qquad (4.2)$$

where $_{y}^{'}$ is the sliding stress at the interface. This model predicts a sliding resistance of 95 MPa at the interface for the limit state, which is close to the computed value of 115 MPa.

The debonded composite has a lower modulus and limit strength than the pristine composite. The value of the initial modulus is approximately half of the value for the pristine composite. This is higher than what is predicted for a stress free interface with no sliding resistance, indicating that some contact is present at the interface for this type of loading. The computations indicate that final limit strength corresponds to a sliding resistance of 55 MPa at the interface, also approximately half the value for the pristine composite. A modest reduction in failure strain that is close to the sample to sample variation is observed.

4.2 Consequences in Design

4.2.1 Stress Redistribution. Titanium matrix composites can be used efficiently in unidirectional lay-ups with the dominating loading in the fiber direction. A MMC ring represents a candidate component that features this type of loading. It has

the fibers oriented in the most highly stressed direction, the hoop direction. For simplicity, the ring will be assumed to be of constant thickness and only loading on the outer radius as seen in Figure 4.3 will be considered. The stress distribution can readily be found in Lekhnitskii [1944] as:

$$\sigma_r = \frac{p}{1-c^{2k}}\left[\left(\frac{r}{b}\right)^{k-1} - C^{2k}\left(\frac{b}{r}\right)^{k+1}\right] \tag{4.3a}$$

$$\sigma_\varphi = \frac{p}{1-c^{2k}}\left[\left(\frac{r}{b}\right)^{k-1} + C^{2k}\left(\frac{b}{r}\right)^{k+1}\right] \tag{4.3b}$$

where $C = \frac{a}{b}$, $k = \sqrt{\frac{E_\varphi}{E_r}}$, a is the inner radius, b is the outer radius and p is the equivalent blade loading on the outer surface. The hoop and radial stress distribution are shown in Figure 4.4 for a ring with a/b = 0.5 and different anisotropy ratios k. The case k = 1.2 corresponds to the elastic properties for the pristine composite and k = 2.1 corresponds to the properties for the debonded composite. The pristine composite has a very low anisotropy and the stress distribution is closely given by the isotropic solution with the highest hoop stress at the inner radius. However, the loss of residual stresses at the interface and the associated debond causes a substantial reduction in the transverse modulus and an increase in the anisotropy of the composite. This alteration causes a dramatic change in the hoop stress distribution and the hoop stress attains its maximum value at the outer radius instead of at the inner radius.

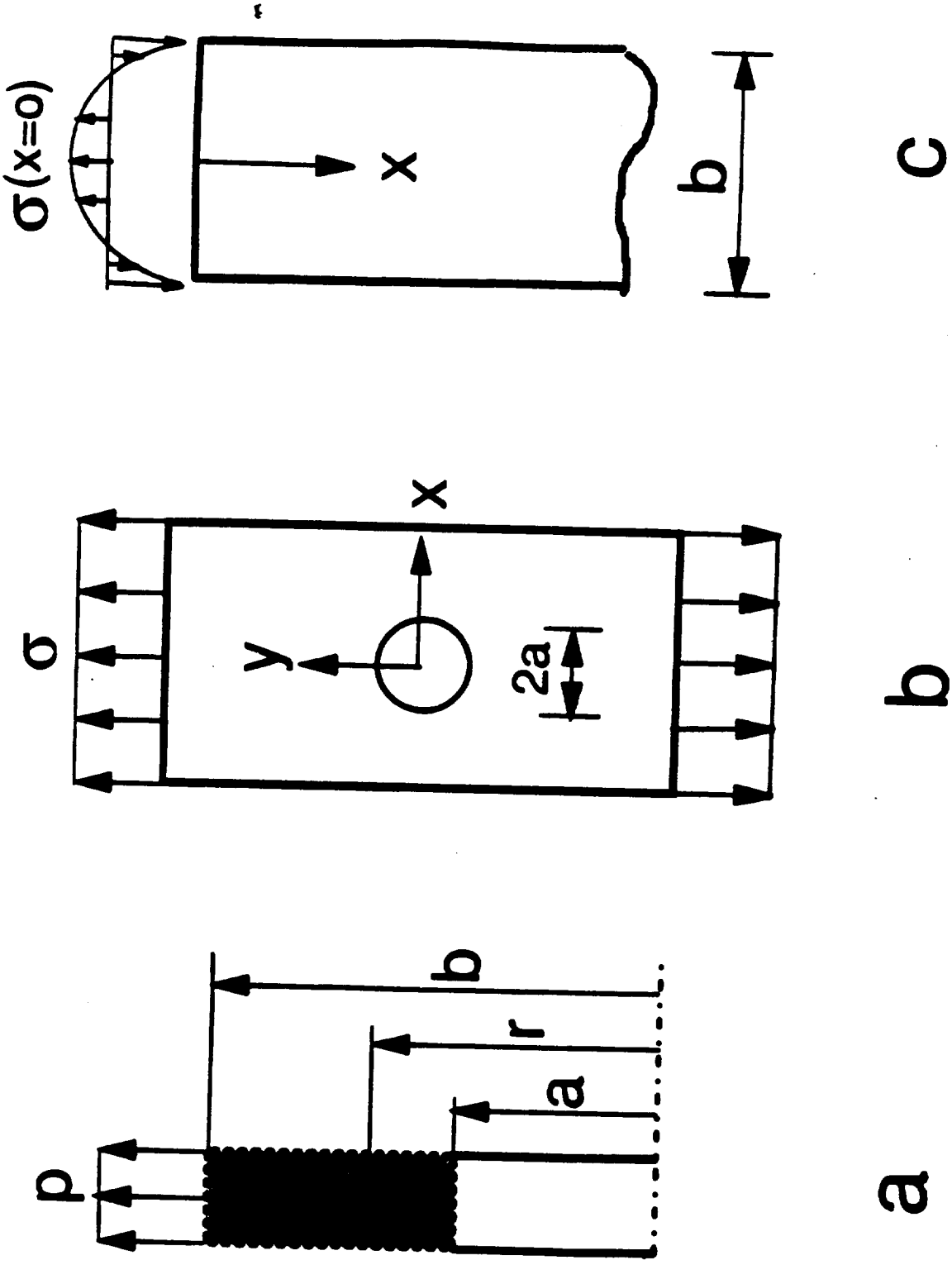

Figure 4.3. Ring geometries and loading conditions for the stress distributions.

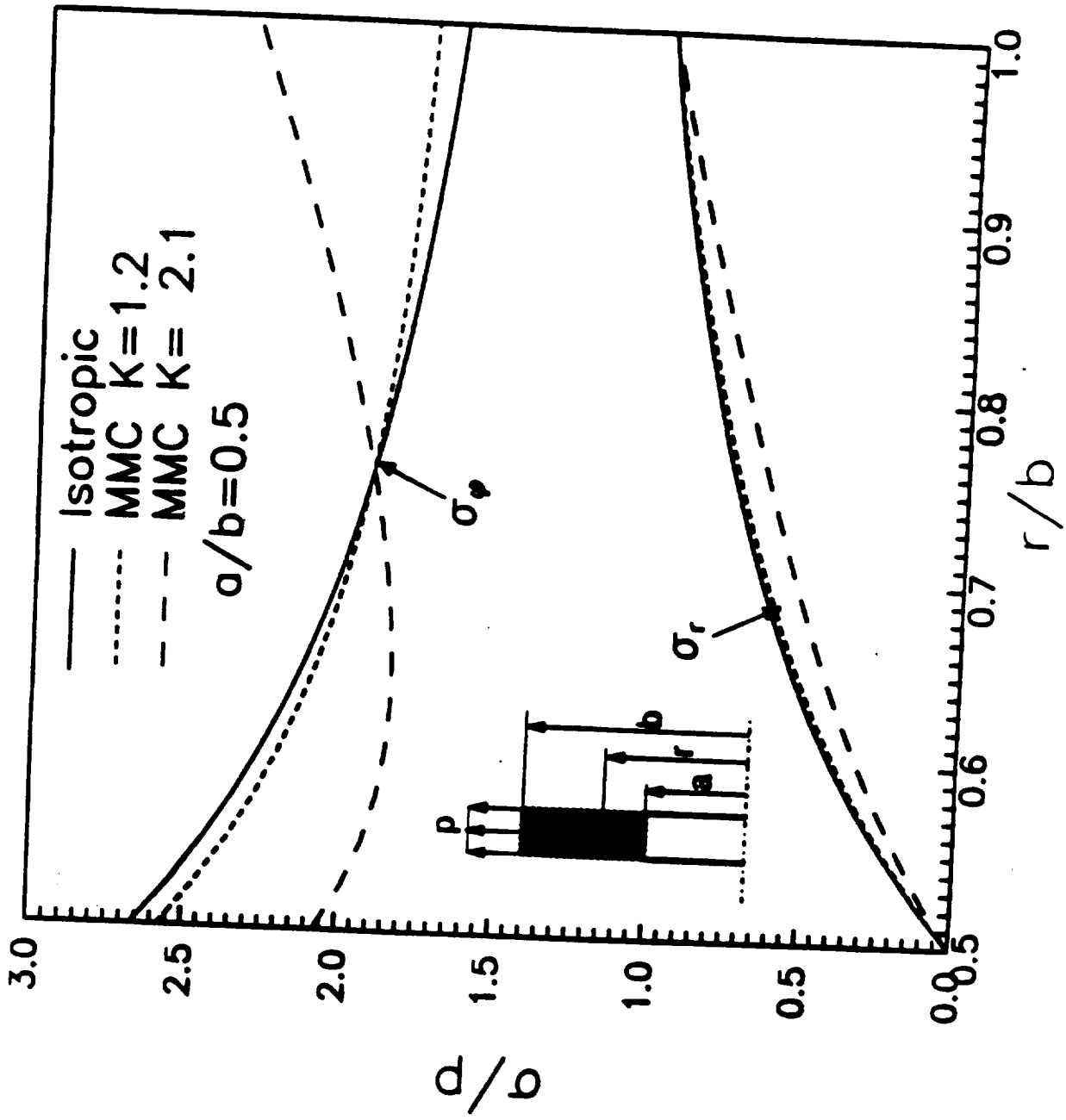

Figure 4.4. Normalized hoop and radial stress distributions for a ring with a/b = 0.5 and different anisotropy ratios k.

The value of the hoop stress at the inner and outer radius are shown in Figure 4.5 for different ring dimensions a/b. It can be deduced that a tremendous stress distribution occurs when the interface debonds for small a/b ratios and the maximum hoop stress can even increase. However, this can be avoided by choosing a larger a/b ratio and it can be seen that the stress redistribution is modest for a/b larger than 0.7. This result implies that this type of stress redistribution can sometimes be avoided by choosing configurations such that the geometry dictates the stress distribution more than the constitutive properties.

4.2.2 Stress Concentration. The highest tensile stress concentration for a hole in a infinite plate illustrated in Figure 4.3b is given by the tensile hoop stress at the ends of the diameter perpendicular to the loading direction, cf. Lekhnitskii [1944], as:

$$\sigma_{Max} = \sigma_y^{\infty}\left[1+\sqrt{2\left(\frac{E_y}{E_x}-\nu_{yx}\right)+\frac{E_y}{G_{yx}}}\right] \tag{4.4}$$

For a pristine composite loaded in the longitudinal direction, the stress concentration is 3.4. After the residual stresses have relaxed at the interface, the stress concentration increases to 4.6. For loading in the transverse direction, the stress concentration for the pristine composite is 2.7 and it decreases to 2.1 for the debonded composite.

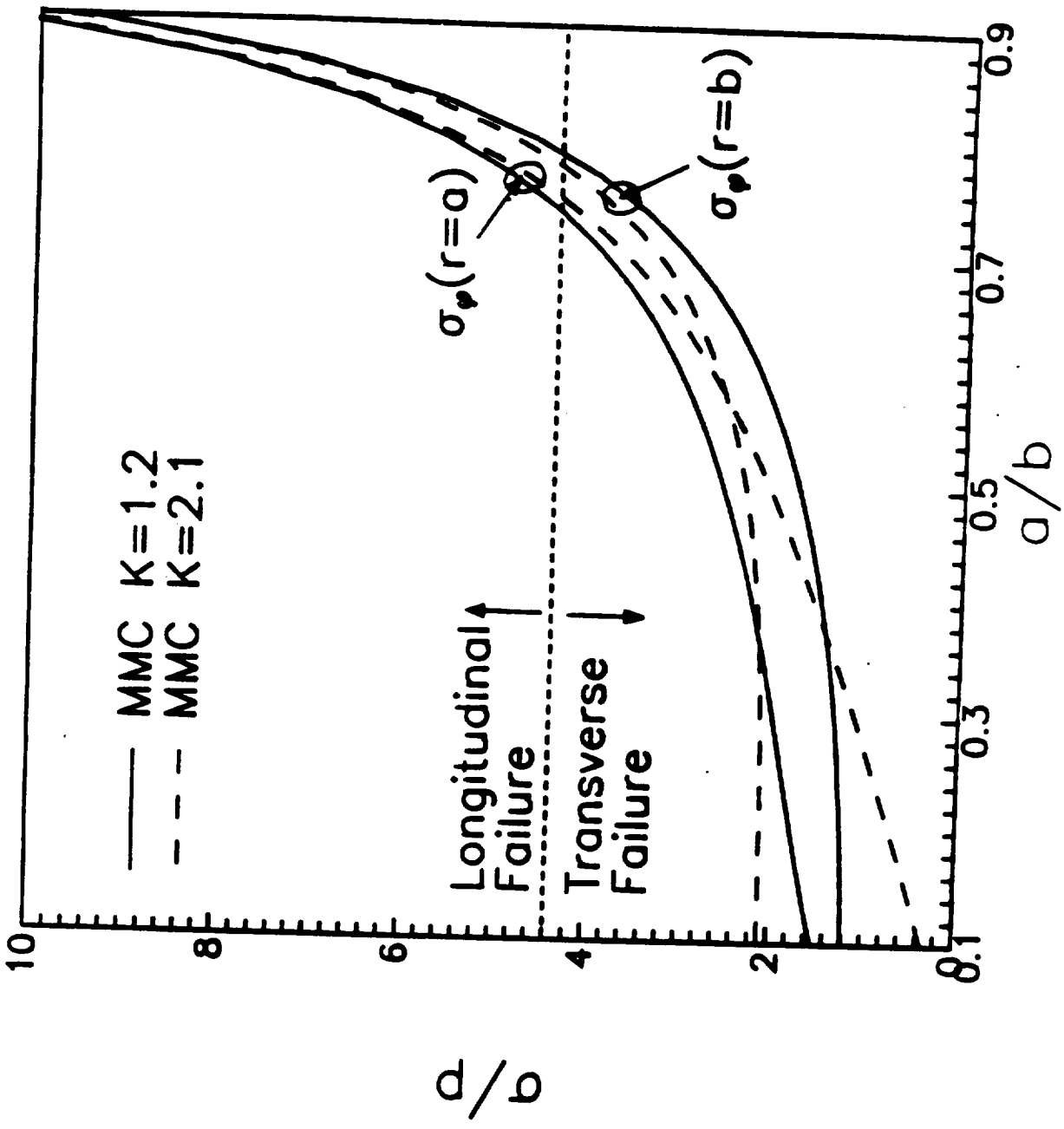

Figure 4.5. The value of the hoop stress at the inner and outer radius for different ring dimensions a/b.

4.2.3 Stress Decay. An interesting issue for composites is how far an edge effect propagates into a component (Saint-Venant's Principle). Edge effects can propagate much farther into highly anisotropic materials than into isotropic materials. This observation was studied by Horgan et al., [1972] for the self-equilibrating loading shown in Figure 4.3c. The approximate stress decay is given by:

$$|\sigma| \leq Ae^{-\lambda x}, x \geq 0 \tag{4.5a,b}$$

where

$$\lambda \approx \frac{2\pi}{b}\sqrt{\frac{G_{xy}}{E_x}} \tag{4.5c}$$

Equation 4.5c indicates that the edge effect has the slowest decay rate in the stiffest direction. For the present composite, the longitudinal modulus can be expected to be unaffected by the debond. An appreciation for the difference in decay rate for the debonded and pristine composite is given by the ratio of the lengths required to achieve the same stress level. Use of equation 4.5c gives:

$$\frac{x^d}{x^p} = \sqrt{\frac{G_{xy}^p}{G_{xy}^d}} \tag{4.6}$$

This implies that the load diffusion length increases by 40 percent for the debonded material.

It has been found that the relaxation of the residual compressive stresses at the fiber-matrix interface causes a reduction in the transverse modulus to a third of the value for the pristine composite.

The initial in-plane shear response is not affected as strongly as the transverse tensile response. The shear modulus is reduced to half of the value for the pristine material. Calculations indicate that the sliding resistance at the interface reduced by half the value of the pristine material. The limit strength in shear is dictated by a combination of the matrix strength and the sliding resistance at the interface. This implies that the limit strength of the composite is only reduced by a factor of 2/3.

Some loadings, such as longitudinal tension, will tend to close the fiber matrix interface and cause the debonded composite to have the same elastic properties as the pristine composite. Other loadings, such as transverse tension, will cause portions of the interface to open up more during loading. This will cause the debonded composite to have elastic properties that are dependent on the loading. Some of the elastic symmetry relations do not apply for constants determined from these different loadings.

It was demonstrated that micro-mechanical simulations can be used as an efficient tool to evaluate the experimental observations. This experience also adds confidence in the use of this approach in predicting composite behavior.

The present titanium materials composite (TMC) systems with weak interfaces are candidates for components with complex shapes. The components will be

manufactured through complex processes and assemblies of sub-components. The individual sub-components can therefore be subjected to a number to thermal cycles with high temperature before service. This can lead to a relaxation of the compressive stresses at the fiber matrix interface. The relaxation leads to a drastic reduction in the transverse modulus. A reduction in transverse modulus causes an increase in the anisotropy of the material, and the stress distribution in a component, consisting of a debonded composite, can be substantially different from the stress distribution for the pristine composite. Hence, design calculations should be performed for the pristine and debonded composite properties to ensure that the component has the required performance.

5.0 CONCLUDING REMARKS & RECOMMENDATIONS

The theoretical research described herein has provided a fundamental foundation for future development and evaluation of aligned fibrous composites for potential application to reinforcing elements for reinforced concrete structures. It has been demonstrated that projecting the structural performance of components from small specimen data to the representative structural level is both volume dependent and configuration dependent. The models and the statistical, Weibull-type theory have been developed to facilitate prediction of the effect of both volume and loading configuration and basic strength properties. Although the research has concentrated to a large degree on a MMC system, with limited discussion of PMC systems and results, the basic mechanics and approaches can be readily extended to PMC systems with much more flexible matrix elastic properties. In fact, we highly recommend that the methods developed here should be further evaluated for realistic fiber and matrix constituents such as E-glass fiber and vinylester matrices.

Emerging from this research is the prospect of translating the key Weibull parameters for individual reinforcing filaments into equivalent Weibull parameters for the unidirectional composite system. Similarly, evaluation of the influence of size (volume) and loading configuration, i.e., tension versus flexure, are also amenable to formal development and assessment. An appropriate blend of materials science and structural mechanics disciplines will be necessary to enable significant scientific and technological advancement of the general application of composites in civil engineering

structural applications. In fact, one of the longer-term goals of our research was to establish a closer interaction with structural engineering. Nevertheless, we strongly recommend that further basic research, of an interdisciplinary nature, should be considered in establishing the groundwork on the mechanisms and characteristics of ductility potential in PMC's with relatively brittle reinforcing filaments. The linkage with the implementation of composites as reinforcing elements as viewed by the structural engineer and concrete technologist is, however, essential in helping to define the role of both reinforcement stiffness, ductility and interface bond/slip between reinforcing elements and concrete at the macro-level. Specific examples would include reinforced and prestressed concrete applications and could, potentially, provide valuable insight for applications-oriented development such as the Advanced Waterfront Technology Test Site (AWTTS) at NFESC (Port Hueneme).

The parallel experimental research has provided insight into both the grip design required to facilitate meaningful test data on candidate rebar tensile behavior as well as an evaluation of the merits of considering development of hybrid rebar configurations. In the former investigation, the local stress distribution in the grip region was determined using finite element analysis and these results indicated the presence of a stress/strain concentration just inside the grip termination location. It was also shown that the layered structure of hybrid rebar tended to significantly modify the stress and strain concentration and resulting distributions in the grip termination region, a factor that potentially contributes to the strength data generated for the rebar specimens.

One of the major difficulties in developing reliable and consistent test data for both grip design and hybrid rebar evaluation the quality of the specimens available. Thus, it is strongly recommended that an alternative source of supply should be explored in ongoing research on grip and rebar experimental evaluations of the type conducted in this research investigation.

Finally, there is a desperate need for a well planned, rigorous assessment of long-term durability and environmental effects on current and future low-cost PMC systems that are candidates for applications in civil engineering in general but, perhaps even more importantly in waterfront or marine structures. Funded research in this area appears quite limited in the United States at present, but environmental concerns remain a major issue for economics/life cycle rationalization.

The UCSB research team is most grateful for the opportunity to conduct this research investigation for NFESC and, despite the need to cut short the originally planned period of research to 2 years, we feel we have gained much from the program and contributed some methodology and data that will prove useful in future research. The expansion of our involvement with the civil engineering community that was fueled by this research involvement has included the NSF Offshore Technology Research Center peer reviews, Federal Highways Advisory Committee on Adhesive-Technology for civil structural applications and Institute of Mechanics and Materials (UCSD) Think-Tank on Durability of Advanced Composites in Civil Structures.

6.0 REFERENCES

Bain, K.R., Byrnes, M.L. and Jain, S.K., 1985, "Fatigue and Fracture of Titanium, Aluminides," Allison Gas Turbine, Indianapolis, Indian, EDR 13084.

Bullock R.E.., 1974, "Strength Ratios of Composite Materials in Flexure and Tension", Journal of Composite Materials," vol. 8, pp. 200-206.

Coleman, B.D., 1958 "On The Strength of Classical Fibers and Fiber Bundles", Journal of the Mechanics and Physics of Solids, vol. 7, pp. 60-70.

Cooper G.A. and Kelly A., 1967, "Tensile Properties of Fiber-Reinforced Metals: Fracture Mechanics," Journal of the Mechanics and Physics of Solids, vol.x, pp.279-297.

Curtin, W.A., 1993, "Ultimate Strengths of Fiber-Reinforced Ceramics and Metals," Composites, vol. 24, pp. 98-102.

Daniels, H.E., 1945, "The Statistical Theory of the Strength of Bundles of Threads-I," Proceedings of the Royal Society, vol. A183, pp. 405-435.

Gundawardena, S., Jansson, S, and Leckie, F.A., 1993, "Modeling of Anisotropic Behavior of Weakly Bonded Fiber Reinforced MMC's," Acta Metallurgica, vol. 41, pp. 3147-3156

Gücer D.E. and Gurland J., 1962, " Comparison of the Statistics of Two Fracture Modes," Journal of the Mechanics and Physics of Solids, vol. 10, pp. 365-373.

He. M.Y., Evans, A.G. and Curtin, W. A., 1993, "The Ultimate Tensile Strength of Metal and Ceramic-Matrix Composites," Acta Metallurgica, vol. 41, pp. 871-878.

Hild F., Domergue J.M., Leckie F. and Evans A. ,1993, "Tensile and Flexural Ultimate Strength of Fiber-Reinforced Ceramic-Matrix Composite," to appear in International Journal of Solids and Structures.

Hild F. and Burr A., 1994, "Localization and Ultimate Tensile Strength of Fiber-Reinforced Ceramic-Matrix Composites," Mechanics Research Communications, vol. 21, pp. 297-302.

Holte, L.E., Dolan, C.W., Schmidt, R.J., "Epoxy Socketed Anchors for Non-Metallic Prestressing Tendons," Fiber-Reinforced-Plastic Reinforcement for Concrete Structures, International Symposium, ACI SP-138, A. Nanni and C.W. Dolan editors, 1993, pp.381-400.

Horgan, C.O., 1972 "Saint Venant End Effects in Composites," Journal of Composite Materials, vol 16, pp. 411-422.

Iyer, S.L., Anigol, M., "Testing and Evaluating Fiberglass, Graphite and Steel Prestressing Cables for Pretensioned Beams," Advanced Composite Materials in Civil Engineering Structures, ASCE Materials Division, S. Iyer and R. Sen editors, Las Vegas, Nevada, January 1991, pp.44-56.

Jansson S., Deve, H.E. and Evans A.G., 1991 " The Anisotropic Mechanical Properties of a Ti Matrix Composite with SiC Fibers," Metallurgical Transactions, vol. 22A, pp. 2975-2984.

Jansson S. and Kedward, K.T., 1994, "Ultimate Tensile Strength of Composites Exhibiting Fiber Fragmentation," to appear in Compositers.

Jansson S. and Leckie, F.A. 1992, "The Mechanics of Failure of Silicon Carbide Fiber-Reinforced Glass-Matrix Composites," Acta Metallurgica, vol. 40, pp. 2967-2978.

Kelly A. and Tyson , 1965, "Tensile Properties of Fiber-Reinforced Metals: Copper/Tungsten and Copper/Molybdenum," Journal of the Mechanics and Physics of Solids, vol. 13, pp 329-350.

Lerch, A.L., Gabb, T.B. and MacKay, R.A., 1990, "Heat Treatment Study of the SiC/Ti-15-3 Composite System," NASA TP 2970.

Malvar, L.J and Bish, J., "Grip Effects in Tensile Testing of FRP Bars," Non-Metallic (FRP) Reinforcements for Concrete Structures, Ghent, Belgium, 1995.

Nedle, M.R. and Wisnom, M.R., 1994, "Stress Concentration Factors Around Broken Fibres in a Unidirectional Carbon Fiber-Reinforced Epoxy," Composites, vol. 25, pp. 549-557.

Neumeister J.M., 1993, "A Constitutive Law for Continuous Fiber Reinforced Brittle Matrix Composites with Fiber Fragmentation and Stress Recovery," Journal of the Mechanics and Physics of Solids, vol. 41, pp. 1383-1404.

Phoenix S. L., 1993, "Statistical Issues in the Fracture of Brittle Matrix Fibrous Composites," Composite Science and Technology, vol. 48, pp. 65-80.

Phoenix S. L, and Raj R., 1992, " Scalings in Fracture Probabilities for a Brittle Matrix Fiber Composite," Acta Metallurgica, vol. 37, pp. 2813-2828.

Sippel, T.M., "Design, Testing and Modeling of an Anchorage System for Resin Bonded Fiberglass Rods used as Prestressing Tendons," Advanced Composite Materials in Bridges and Structures, First International Conference, K.W. Neale and P. Labossiere eds., Sherbrooke, Quebec, Canada, 1992, pp.363-372.

Sutcu M., 1989, "Weibull Statistics Applied to Fiber Failure in Ceramic Composites and Work of Fracture," Acta Metallurgica, vol. 37, pp. 651-661.

Thouless, M.D. and Evans, A.G.,1988 " Effect of Pull-Out on the Mechanical Properties of Ceramic Matrix Composites," Acta Metallurgica, vol. 36, pp. 517-522.

Weibull W., 1939, "The Phenomenon of Rupture in Solids," IVA Proceedings, Stockholm, No 153.

Whitney J.M. and Knight M., 1980, "The Relationship Between Tensile Strength and Flexure Strength in Fiber-Reinforced Composites," Experimental Mechanics, vol. 15 ,pp. 211-216.

Zweben, C. and Rosen, B.W., 1970, " ," Journal of the Mechanics and Physics of Solids, vol. 18, pp. 189-206.